Applications of Raman spectroscopy, a tool to investigate glass structure and glass fiber

D R Neuville, M R Cicconi, W Blanc, M Lancry

Applications of Raman spectroscopy, a tool to investigate glass structure and glass fiber

D.R. Neuville[1], M.R. Cicconi[1], W. Blanc[2], M. Lancry[3]

[1] *Géomatériaux, CNRS-Institut de Physique du Globe de Paris, Paris University*
1 rue Jussieu, 75005 Paris, France
neuville@ipgp.fr
[2] *Université Côte d'Azur, CNRS, Institut de Physique de Nice (INPHYNI), UMR7010, Avenue Joseph Vallot, 06108 Nice, France*
wilfried.blanc@inphyni.cnrs.fr
[3] *Institut de Chimie Moléculaire et des Matériaux d'Orsay (ICMMO), Université Paris-Sud, Université Paris Saclay, CNRS, Orsay, France*
matthieu.lancry@u-psud.fr

1. Introduction

Since Raman spectroscopy was discovered, in 1928, it has been recognized as an important analytical tool with high potential, due to its non-destructive nature and its ability to provide information in a wide variety of fields like physics, chemistry, earth sciences and biology. Similarly, in everyday life or in several crime TV series, scientific policemen use a portable Raman spectrometer to analyze the crime zone. However, its greater instrumental complexity, in comparison to infrared spectroscopy, delayed its implementation outside research laboratories especially in industrial environments. If Raman spectroscopy is named after C.V. Raman (Nobel Prize in Physics, 1930), several groups between 1920-1930 worked on this subject around the world: 1) an Indian group composed of Raman and Krishnan (1928), who made the first observations of the phenomenon in liquids in 1928; 2) Landsberg and Mandelstam (1928) in the USSR reported the observation of light scattering with change of frequency in quartz and finally 3) Cabannes and Rocard (1928) in France, theoretically confirmed the Raman and Krishnan observations, and in the same year Rocard (1928) published the first theoretical explanation.

Today, Raman spectroscopy is a commonly used technique, the development of which was often associated with technological progress. Figure 1 shows the number of publications over time, clearly showing that its use directly correlates to technological developments (laser, CCD confocal system). The most recent increase of the number of publications per year results from the decreasing cost of Raman spectrometers (lowest price around 1000$ up to a triple spectrometer for 200000$). Raman spectroscopy is a very important practical tool for quickly identifying molecules and minerals. For example, a Raman spectrometer was deployed on the Viking landers in 1972 and on other missions (Angel et al. 2012) and more recently in deep ocean exploration (Zhang et al. 2012). Raman spectroscopy also has important scientific applications in medical diagnostics (Tu and Chang 2012) and probably soon, the next Martian missions will be equipped with portable Raman installed on rovers (Di Genova et al., 2016).

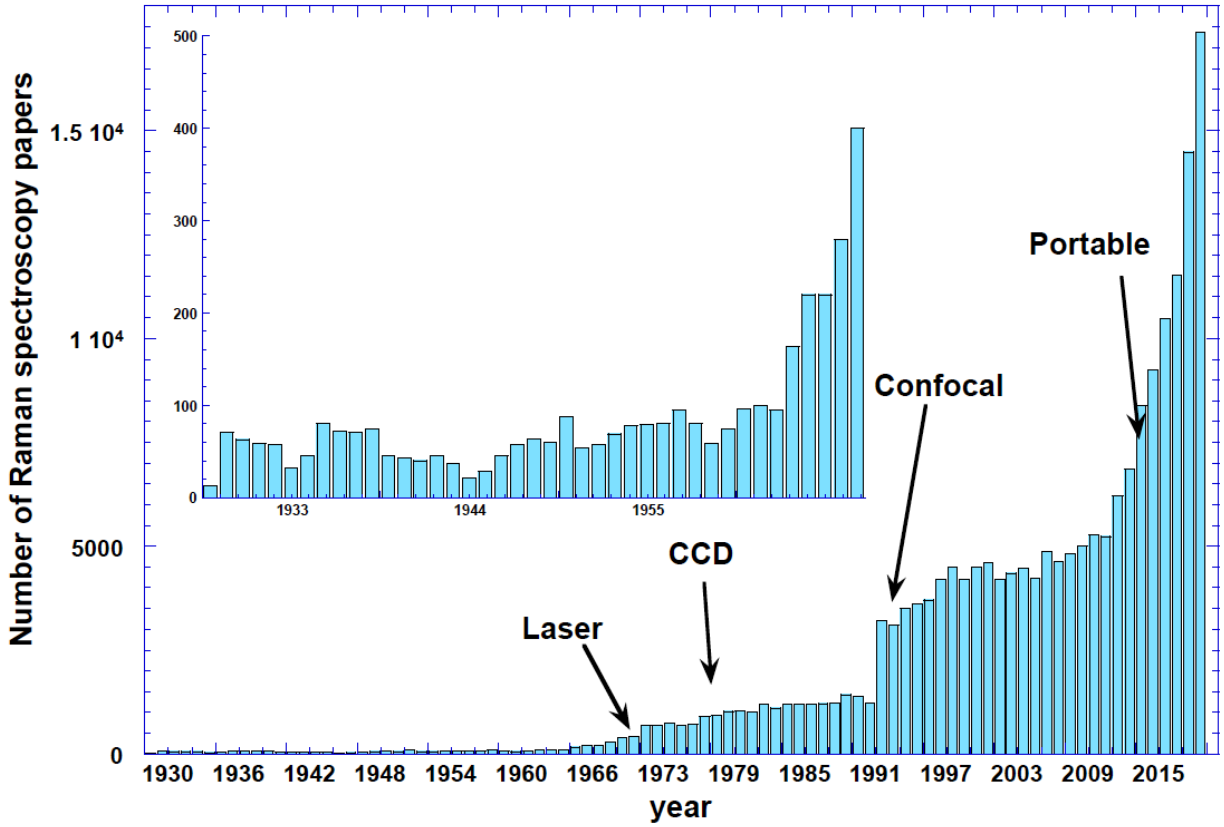

Figure 1: Number of scientific paper published per year between 1929 and 2018.

The first Raman articles cover all subjects: liquids, gases, organic matter and even glasses. The first two papers on glass structure using Raman spectroscopy were done by Hollaender and Williams (1929, 1931), just a few years before the X-ray diffraction studies of Warren (1934a, b). In particular, Hollaender and Williams (1929, 1931) noticed similarities between the bands of crystalline quartz observed by Landsberg and Mandelstam (1928) and those observed in fused silica even if the latter were slightly broader and less contrasted. These promising beginnings explain why, nowadays, Raman spectroscopy is widely used for material characterization both in academic research and in industrial processes.

In this chapter, we will show the relevance of Raman spectroscopy for the study of amorphous materials, but also, we will provide an overview of applications on crystallites and on the use of Raman spectroscopy to monitor nucleation and growth processes. The reader is also referred to some general texts on vibrational properties (Herzberg 1945a; Wilson et al. 1955; Harris and Bertolucci 1978), Raman spectroscopy (Herzberg 1945b; Sherwood 1972; Lazarev 1972; Long 1978, 2002), and applied Raman spectroscopy (Karr 1975; Dubessy et al. 2012) for a more detailed understanding of the technique. We do however briefly discuss techniques such as Hyper-Raman spectroscopy (HRS) and surface enhanced Raman spectroscopy (SERS). Recent reviews of Raman spectroscopy have been made by Nasdala et al. (2004), Das and Agrawal (2011), and Neuville et al. (2014), on Hyper-Raman spectroscopy (Ziegler 1990), SERS (Fleischmann et al., 1974; Jeanmaire and Van Duyne, 1977; Albrecht and Creighton, 1977; Stiles et al. 2008; Cialla et al. 2012; Haidar et al., 2015, 2016), and coherent anti-stokes Raman spectroscopy (CARS) (Maker and Terhune 1965, Begley et al., 1974; Cheng 2004).

2. Brief historical perspective and simple theory

The so-called Raman effect describes the changes in the radiation frequency when a monochromatic light interacts with a substance. When monochromatic radiation ν_o, is incident on a system (in any physical state) most of the radiation is transmitted through the system without interacting with it. Only some of the radiation is scattered. This light mostly has the same frequency as the incident light. Only a small amount presents a change in the frequency. The frequency of the scattered radiation corresponds to $\nu' = \nu_o \pm \nu_m$. In molecular systems, the frequency of the Raman-active vibration (ν_m) is found to lie principally in the range associated with transitions between vibrational, rotational and electronic energy levels (*cf.* Neuville et al. 2014).

The principle of Raman spectroscopy is the illumination of a material (either bulk, powder, or fiber) with a beam of monochromatic light (laser) in the visible spectral range followed by the interaction of the incident photons with the molecular vibrations or crystal phonons, which induces a slight shift in the wavelength of the scattered photons. Scattering can occur with a change in vibrational, rotational or electronic energy of a molecule. When the scattered radiation has the same frequency as the incident light, the scattering is elastic (Rayleigh scattering) and this is the predominant interaction. In contrast, the scattering is called inelastic when the scattered photons have a different frequency (Raman scattering) and the scattered photons exhibit a shift in energy called the Raman shift. However, the Raman shift only occurs when the electron cloud, between the vibrating atoms involved in the interaction with the incident light, is able to be deformed. This deformation is described as the polarizability of the molecule or bond. A change in the degree of polarization potential or polarizability with respect to the vibrational coordinates of the system being studied is required for a molecule to exhibit the Raman effect. The frequency or energy shift can then be measured by a spectrometer. The spectral shift or Raman shift (given in cm^{-1} where $\Delta\nu = (1/\lambda_0 - 1/\lambda_m)$: ν is the Raman shift expressed in wavenumber, λ_0 is the laser wavelength and λ_m the Raman spectrum wavelength) corresponds to the vibrational frequency of the vibrational source (molecule, molecular/atomic group) and is characteristic of the atoms undergoing vibration. The relative intensity of the Raman peaks or bands depend upon the nature of the scattering material and the type and concentration of the atoms undergoing vibration (specifically to the molecule or bond polarizability).

In other words, monochromatic laser light with frequency ν_o excites molecules and transforms them into oscillating dipoles the magnitude of which is related to the degree of polarizability. Such oscillating dipoles cause the interacting photons to be scattered with three different frequencies (schematically represented in Figure 2):

- A molecule with no Raman-active modes (vibrations) interacts with a photon with frequency ν_o. The excited molecule returns back to the same basic vibrational state and scatters light with the same frequency ν_o as the excitation source. This type of interaction is elastic Rayleigh scattering.
- A photon with frequency ν_o interacts with a Raman-active molecule, which, at the time of interaction, is already in the excited vibrational state. Excessive energy of excited Raman-active mode is released, molecule returns to the basic vibrational state and the resulting frequency of scattered light goes up to $\nu_o + \nu_m$. This Raman frequency is called "Anti-Stokes".
- A photon with frequency ν_o interacts with a molecule, which at the time of interaction is in the basic vibrational state. Part of the photon's energy is transferred to the Raman-active vibration with frequency ν_m and the resulting frequency of scattered light is reduced to $\nu_o - \nu_m$. This Raman frequency is called Stokes frequency, or just "Stokes".

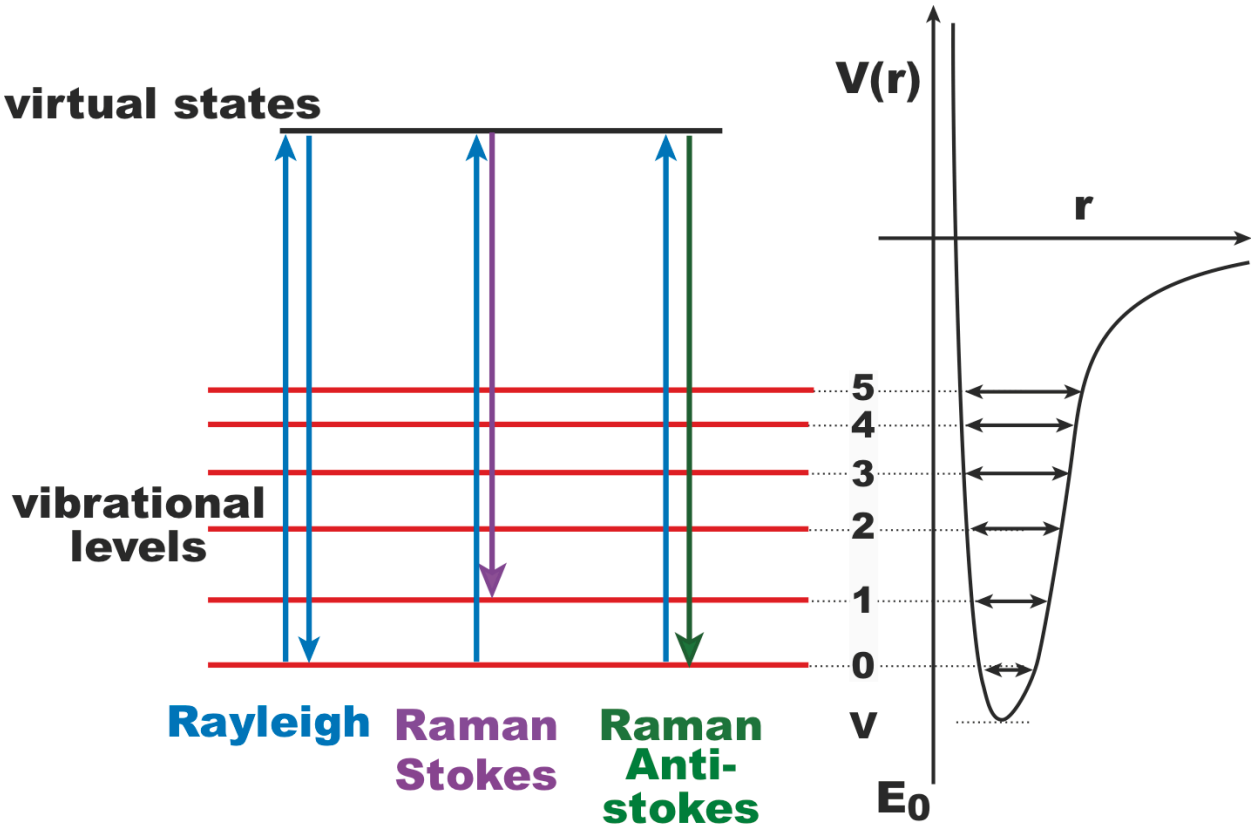

Figure 2: Virtual states versus vibrational levels.

If the investigated material is illuminated by monochromatic light, for example with a laser, the spectrum of the scattered light consists of a strong line (the exciting line, Fig 3a) of the same frequency as the incident illumination together with much weaker lines on either side shifted from the strong line by frequencies ranging from a few to about 4000 cm^{-1} (Fig. 3a,b). The higher the frequency, lighter are the atoms involved in the molecular vibration. In the figure 3b, the vibrations of a H_2 molecule at 3500 cm^{-1} is not shown.

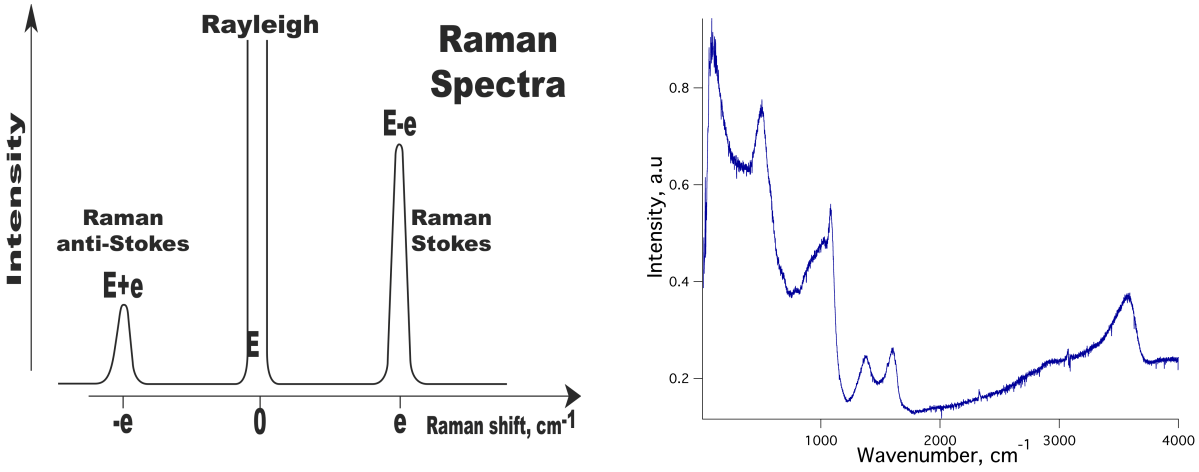

Figure 3: a) Schematic of the exciting line, at 0 cm^{-1}, and the Raman scattering on the left and right, Stokes and Anti-stokes Raman frequencies, respectively. b) Raman spectrum of a hydrous aluminosilicate

glass. Different regions can be observed in the spectrum that can be assigned to different types of vibrations b) the Boson peak (20-200cm^{-1}), Al-Si-M vibrations (200-700 cm^{-1}), Si-Al stretching vibrations (700-1200 cm^{-1}), Non-Bridging oxygen (NBO) vibrations (900-1200 cm^{-1}) and H_2O-OH stretching vibrations (1300-1600 cm^{-1}, 3000-4000 cm^{-1}).

Classical theory

Raman scattering occurs when monochromatic light interacts with molecular vibrations or crystal phonons (vibrations propagating along the crystallographic axis). To a first approximation (the so-called harmonic approximation), the vibration can be modeled by a spring binding two masses (m_1 and m_2) with a force constant k. The vibrational frequency, corresponding to the eigen mode of vibration of the spring, can be calculated as: $\nu=1/2\pi(k/\mu)^{1/2}$ with μ, the reduced mass ($\mu=m_1.m_2/(m_1+m_2)$).

The vibrational frequency depends on several physical and chemical parameters: the chemical nature of the atoms involved in the bond, the nature of the bond (modeled by the force constant, k) and the symmetry of the molecule or molecular group undergoing the vibration. Thus, the vibrational frequency can be considered as a characteristic signature of the material being studied. Indeed, each specific molecule or crystal has its own vibrational frequencies and can be characterized and identified by using these frequencies. Raman spectroscopy enables one to measure these fundamental vibrations resulting in sharp, well-resolved bands visible in a Raman spectrum of a gas or crystalline material.

Several books are available on the subject from theory to applications (Herzberg, 1945a,b; Wilson et al., 1955; Sherwood 1972; Lazarev 1972; Long 1977, 2002; Harris and Bertoluci, 1978).

3. Instrumentation

By looking at one of the first Raman spectra of ground glass from Raman and Krishnan (1929) obtained by using a mercury arc lamp as excitation source (Figure 4), it is easy to realize that progress in Raman spectroscopy has been directly correlates to technological developments of excitation sources, detectors, and so on (e.g. lasers, charge coupled devices (CCD), laser optics).

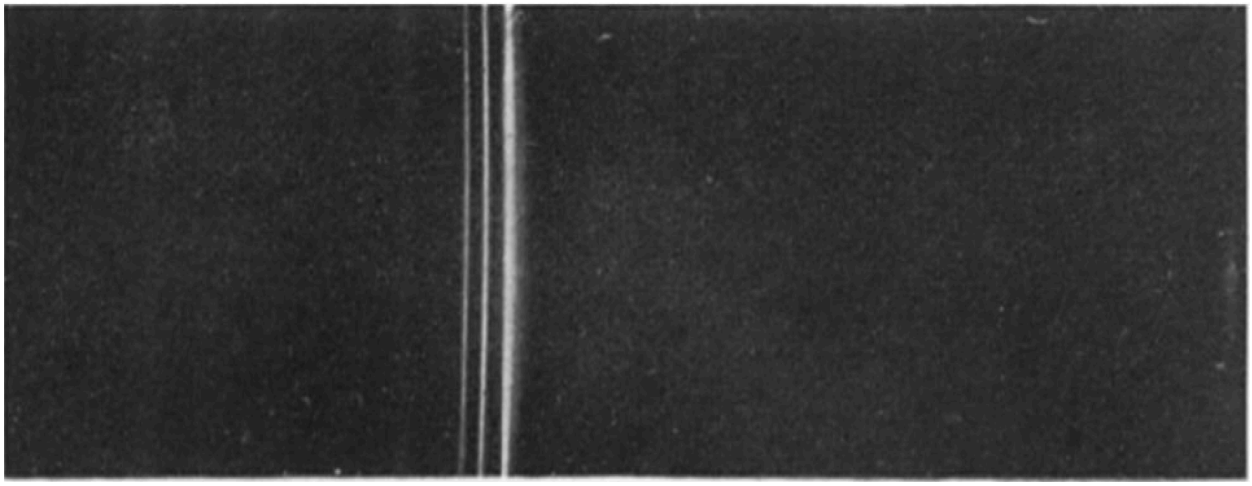

Figure 4: Spectrum of the λ 4358 group of lines of the mercury arc, scattered by a plate of ground glass. *(from Raman and Krishnan, 1929).*

After discovery of the Raman effect and production of the first Raman spectra between 1928 and 1935, papers on Raman spectroscopy were focused on theory (Cabannes, 1928; Rocard, 1928),

on crystals (Landsberg and Mandelstam, 1928), liquids (Raman and Krishnan, 1929, Cabannes et Rousset, 1932; Hibben, 1933, 1936), gases (Mulliken, 1929, 1931) organic matter (Villars, 1932; Hibben, 1933), and on glasses (Hollaender and Williams, 1929, 1931) with less than 50 papers published per year. Since then the technique has rapidly grown (Figure 1) with applications across all scientific disciplines from physics to medicine to archeology and anthropology. The last big increase in the number of scientific publications in 2011 (Figure 1) corresponds to the huge decrease of the prize of Raman instruments and also to the development of new portable Raman spectrometers.

3.1 Excitation line

During the first 30 years of Raman development, Raman spectra were obtained by exciting material using generally a mercury vapor arc lamp. In the 1950's, Kastler and co-workers (Nobel Prize, 1966) developed the laser (Light Amplification by Stimulated Emission of Radiation) and since the 1960's, a sample is normally illuminated with a laser beam in the ultraviolet (UV), visible (Vis) or near infrared (NIR) range. A laser is a device that emits light (electromagnetic radiation) through a process of optical amplification based on the stimulated emission of photons. The emitted laser light is notable for its high degree of spatial and temporal coherence. Laser beams can be focused to very small spots, achieving very high irradiance. Or they can be focused into a beam with low divergence in order to concentrate their power at longer distances.

Laser light is theoretically a single wavelength but a laser actually produces radiation in several modes having slightly different frequencies, often with more than a single polarization. Consequently, in order to carry out Raman experiments one may have to tune the Laser frequency appropriate for the experiment and/or employ some sort of wavelength filter (Plasma Filter) to produce the ν_0 necessary for the experiments. In addition, the laser chosen for an experiment needs to be appropriate for the type of material being studied. For example, colored samples may absorb rather than scatter certain laser wavelengths and so one needs to choose a laser wavelength that minimizes absorption (Table 1). Nowadays, the new Raman systems benefit from the miniaturization of new lasers, which could even be as small as a pen.

Table 1: Typical laser wavelengths from near-IR to UV.

Wavelength (nm)	Sample type
830	biological
785	polymers, biological & general purpose
633	corrosion materials & general purpose
532	minerals, glass, general purpose and Raman portable
514 & 488	semiconductors, catalysts, biological, polymers, minerals, glass, general purpose
325	wide band gap semiconductors
244	biological, catalysts (Resonance Raman)

3.2 Notch filters, optical spectrometer or grating, monochromators?

During a Raman experiment scattered light is collected with a lens and is sent through an interference filter or spectrophotometer. Since spontaneous Raman scattering is very weak the main difficulty of Raman spectroscopy is separating the scattered light from the intense Rayleigh scattering (ratio $1/10^9$). Thus, the Rayleigh scattering must be separated from the Stoke or anti-Stoke lines because their respective intensities have several orders of magnitude of difference, and the Rayleigh signal completely masks the signal of the other lines. There are two possibilities to remove or minimize the strong Rayleigh line, either using several gratings to better separate the lines or using filters to cut the Rayleigh:

- -i) cutting off the spectral range close to the laser line where the stray light has the most prominent effect. People use commercially available interference (Notch®) filters which cut-off spectral range of ± 10-120 cm^{-1} from the laser line. This method is efficient for stray light elimination but it does not allow detection of low-frequency Raman modes in the range below 100 cm^{-1}. Notch® filters are also very expensive and a different filter is required for each Laser excitation line. The simplest method to eliminate or reduce the Rayleigh scattering is to use a grating (100 line/mm) in front of the laser to remove parasitic lines from the laser as well as the Rayleigh scattering. Another possibility is to use a prism spectrometer to separate the Rayleigh and parasite line. These two methods are cheaper than buying several Notch® filters and are adjustable depending on the excitation line. In all cases, whichever method is employed, Notch® filter, prism spectrometer or grating, there is a decrease in efficiency with age and/or power of the Laser. Stray light is generated in the spectrometer mainly from light dispersion on gratings and strongly depends on grating quality. Modern Raman spectrometers typically use holographic gratings, which normally have fewer manufacturing defects in their structure then older line gratings. The stray light produced by holographic gratings is about an order of magnitude less intense then from ruled gratings with the same groove density.

- ii) Another way of stray light reduction is to use multiple dispersion stages. Double and triple spectrometers allow measurement of Raman spectra without use of notch filters. In such systems Raman-active modes with frequencies as low as 0.5cm^{-1} can be efficiently detected. This sort of apparatus is generally marketed under the name of triple spectrometer such as Jobin-Yvon-Horiba T64000 spectrometers.

Figure 5 shows Raman spectra on the same glass sample made with a T64000 Jobin-Yvon with one and three gratings for the same acquisition time. Raman spectra obtained with only a single grating spectrometer are three times more intense than those made with a triple grating spectrometer. Note the low frequency spectral cutoff is around 250 cm^{-1} for the single grating but < 5 cm^{-1} for the triple grating. The low frequency cutoff for a single grating instrument depends directly on the nature of the Notch® filter used and its age. Spectral resolution is also three times better with the triple spectrometer than with a simple grating (generally between 7 and 20 cm^{-1} for a simple and up to 0.5 cm^{-1} for a triple spectrometer).

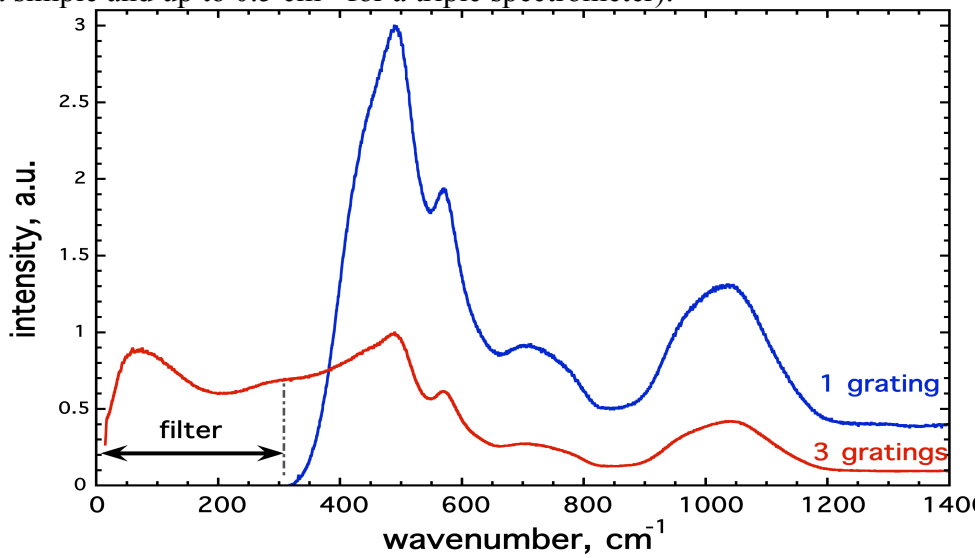

Figure 5: Raman spectra collected with one and three gratings, for the same glass, and using equal acquisition times.

3.3 Detectors

In earlier times people primarily used single-point detectors such as photon-counting Photomultiplier Tubes (PMT). However, a single Raman spectrum obtained with a PMT detector in wavenumber scanning mode was taking a substantial period of time, slowing down any research or industrial activity based on the Raman analytical technique. Nowadays, more and more often researchers use multi-channel detectors like Photodiode Arrays (PDA) or, more commonly, a Charge-Coupled Devices (CCD) to detect the Raman scattered light. Sensitivity and performance of modern CCD detectors are rapidly improving. Most of the times, a CCD is become the detector of choice for Raman spectroscopy since it is extremely sensitive to light.

Thanks to technology progresses, nowadays it is easy to find Peltier cooled detectors that have two main advantages: 1) do not require the use of liquid nitrogen 2) are much smaller, and relatively lighter (< 500 grams). These two characteristics have been of central importance in the development of the new small Raman spectrometers.

3.4 Confocal system

Confocal microscopy is an optical imaging technique used to increase optical resolution and contrast of an image by using a spatial pinhole to eliminate out-of-focus light in specimens that are thicker than the focal plane.

The original idea was developed by Minsky in 1961 and adapted for Raman spectrometers (Figure 6) by Dilor in the early 1990s, now part of the Horiba group. This technique has gained popularity in the scientific and industrial communities and in particular in Raman spectroscopy. The laser beam illuminates the sample via the pinhole (D1), which limits the spacial resolution. The backscattered light, then passes through a beamsplitter which passes the scattered light through a second pinhole (D2). The second pinole has a diaphragm, which is adjustable between 1 micron up to more than 10 microns diameter with a 100x objective lens. The advantage of having the adjustable pinhole is that one can adjust the volume of the sample from which the scattered light is being collected.

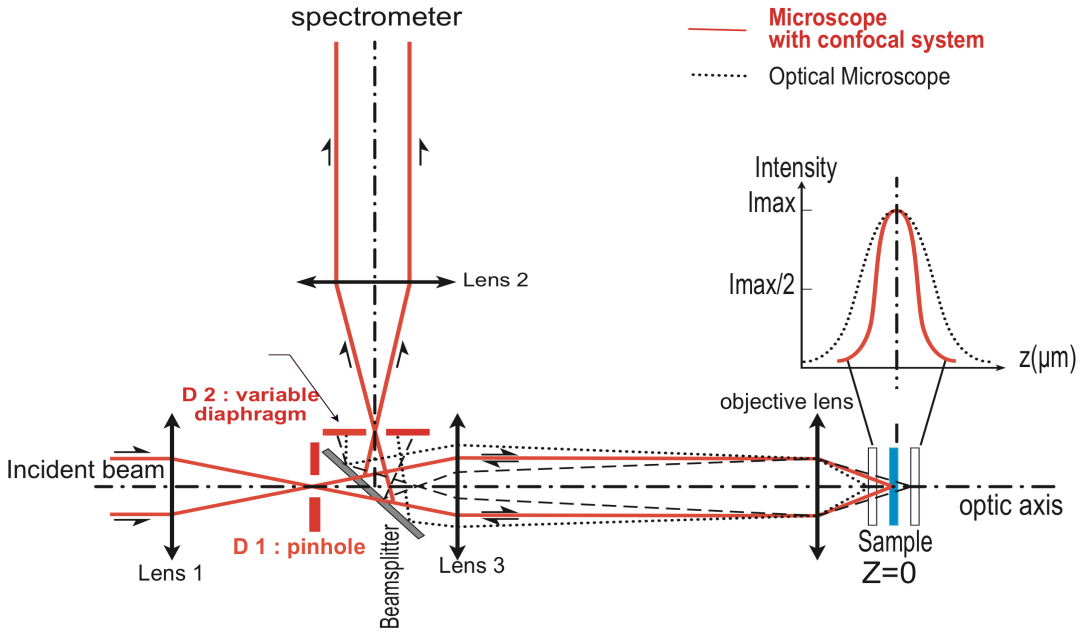

Figure 6: Confocal system on a Raman spectrometer.

3.5 Data acquisition and reduction

Raman spectra quality depends on:

- i) experimental parameters from the spectrometer (quality of lens, grating, detector, beamsplitter);
- ii) size of confocal hole;
- iii) magnification and numerical aperture of the microscope objectives;
- iv) excitation line, λ_0;
- v) sample surface;
- vi) colored or uncolored sample compared to λ_0;
- vii) sample heterogeneity;
- viii) refractive index of sample;
- ix) micro Raman in VV and VH polarization.

Since the 1990's, an optical microscope is generally used to focus the laser spot onto the material surface. The zone sample analyzed depends on several factors such as the opening of the confocal diaphragm, the nature of the sample and the excitation line. The size of the spot is defined by the objective and by the closure of the confocal hole. It must be estimated on each Raman spectrometer by using forms of sizes known for the definition of the side size. The nature of the sample is going to force its refractive index and absorption. We can define two important parameters: Depth of field (*d.o.f*) and the diameter of the analysis spot (*D*):

$$d.o.f = 4\,\lambda/Ob^2$$

Where *Ob* represents the digital opening of the objective, *Ob*, and λ the excitation wavelength.

The diameter *D* of the spot can be estimated by using the Rayleigh criterion on the Airy function:

$$D=1.22\lambda/Ob$$

The scattered light is collected by the same objective (backscattering configuration) and the size of the analyzed volume is determined by the confocal hole of the microscope.

Commonly, Raman spectra on crystalline phase are obtained in a few seconds with at least three scans, in order to ensure a good signal to noise ratio. Modern data collection software automatically correct spectra for non-reproducible signals (e.g. cosmic lines) if more than two spectra are collected under the same instrumental conditions. However, for amorphous solids and liquids, the acquisition time can significantly increase depending on the signal to noise required, even up to 600s per scan window. Futhermore, for some experiments the number of repeat scans may also need significantly increasing to >30 repeat scans. Conditions requiring such long acquisition times may be due, for example, if the experiment requires very low laser power so as not to induce damage to the sample e.g., hydrated iron-phyllosilicate, Gillet et al., (2001), or when examining low concentration elements within the sample e.g., dissolved volatiles elements (Thomas et al., 2000).

The analyzed volume is usually adjusted to be close to the surface in the optimum region for the maximum Raman signal, i.e., within the first 10 µm of depth (Behrens et al., 2006). Effects of focusing depth on the results are very important for colored glasses like iron. Figure 7a,b show Raman spectra of an uncolored glass (Fig 7a) and a black glass (Fig 7b), for which the depth effect is clearly visible. In the case of transparent glass, Raman spectra do not change between surface

up to 200 µm depth whereas a strong decrease of the signal is clearly visible for the black glass between 0 and 60 µm (Fig 7b).

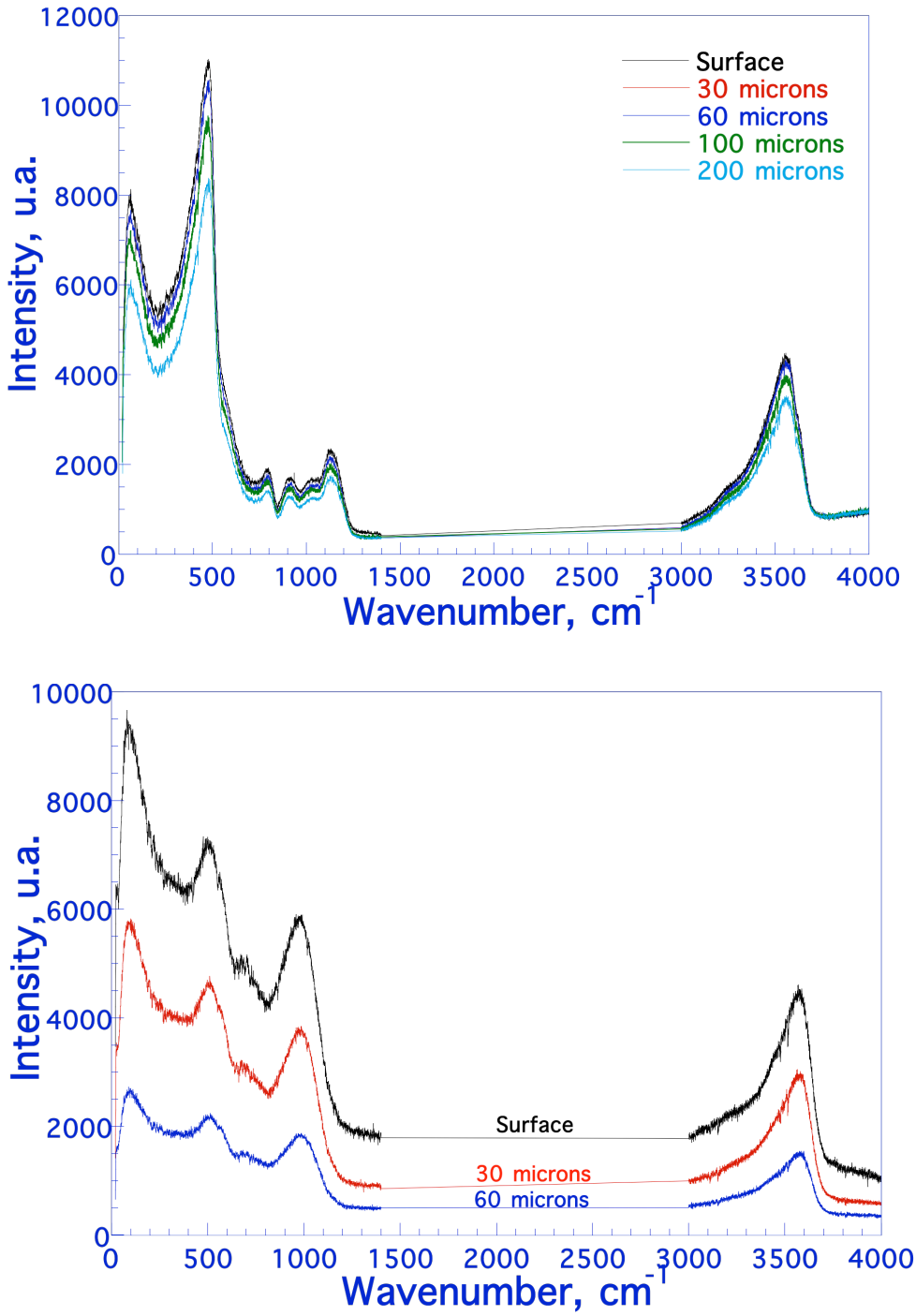

Figure 7: Raman spectra of uncolored glass, (a) and colored glass (b) as a function of depth.

This phenomenon has been attributed to a variation in optical transmission as a function of the wavelength through the crystal. However, Behrens et al. (2006) did not report any change in Raman spectra due to the focusing depth in iron-free glasses, at least up to 200 µm. Focusing effects are discussed in detail in Behrens et al. (2006). For uncolored samples, focus does not modify Raman spectrum while for colored samples Raman intensity decreases as a function of the cross section of the coloring cations.

Raman scattering has two components (two polarization directions), one parallel and one perpendicular to that of the incident light. To acquire Raman spectra, it is possible to exploit this characteristic to provide useful information about the material orientation and symmetry. By using polarized light, only part of the Raman modes will be active, depending on the symmetry of the molecule investigated. In isotropic materials, like glasses, the use of polarized light provides important information on the symmetry of bond vibrations. For example, recently, Helhen and Neuville (2015) have shown that by collecting parallel polarized (VV) and cross-polarized (VH) Raman spectra it is possible to get insights on the element role within the glass network. Indeed, the authors were able to define the behavior of alkaline and alkaline-earthand discriminate their role as network modifier and/or charge compensator in silicate glasses.

3.6 Temperature and excitation line effects.

Raman spectra can change as a function of excitation line and temperature. Both effects have been described and discussed in detail in different books and papers (Shuker and Gammon, 1970; Long 1977; Galeener and Sen, 1978, Seifert et al., 1982, McMillan et al., 1984, Neuville and Mysen, 1996; Helhen, 2010). In earth sciences, one of the most commonly used equations is provided by Long (1977), and several authors have used the correction given below to compare glass Raman spectra taken at different temperatures and with different exciting lines (Mysen et al., 1982; McMillan et al., 1994; Neuville and Mysen, 1996).

$$I = I_{obs} [\nu_0^3 [1-\exp(-hc\nu/kT)] \nu/ (\nu_0-\nu)^4],$$

where h is the Planck constant (6.626038×10^{-34} Js), k is the Boltzmann constant (1.38066×10^{-23} JK^{-1}), c is the speed of light (2.9979×10^{10} ms^{-1}), T is the absolute temperature (K), ν_0 is the wavenumber of the incident laser light, and ν is the measured wavenumber (cm^{-1}) (Long, 1977). This correction allows comparison of glass spectra taken with different incident excitation lines, and/or comparison of spectra acquired at different temperatures, such as in the case of *in-situ* measurements.

The correction stems from initial studies of glasses, which exhibited an apparent temperature dependence of the low frequency bands (Hass, 1969). Hass (1969) showed that for vitreous silica the region below 300 cm^{-1} was strongly affected by temperature. However, above 300 cm^{-1} the affect was essentially negligible. This temperature dependence was attributed to temperature effects on the thermal population of the initial vibrational states. The initial part of the "Long" correction ($[\nu_0^3 [1-\exp(-hc\nu/kT)]$) accounts for these so-called thermal effects. Prior to the mid to late 80's the low frequency Boson peak was not effectively recognized as being a real feature in the Raman spectra of glasses. The intensity attributed to "thermal effects" by Hass (1969,1970) is in fact the Boson peak so that application of the "Long" correction effectively eliminates the Boson peak from the data. In addition, in nearly all papers published in the 60s and 70s on the thermal effect, the authors took a lot of effort to point out that these thermal effects are limited to the low frequency region of the spectra and should not be applied beyond ~300 cm^{-1} (Hass, 1970; Shuker and Gammon, 1970). The second part of the "Long" correction takes into account contributions to the intensity from the exciting line that as well is only applicable to the low frequency regions of the spectra.

3.7 Baseline correction and normalization

In order to compare several Raman spectra, it is important to normalize the spectra and to use a common baseline correction. Several authors normalize Raman spectra to the maximum intensity (see Mysen and Frantz 1992, 1993, 1994a,b; McMillan 1984; McMillan et al. 1994). This is very

easy to do and generally gives good results unless one wants to compare the low frequency region. In this case, it is better to divide the intensity of the Raman spectra by the power of the laser and the acquisition time to obtain a spectrum in 1 s and 1 mW (Neuville 2006). To investigate redox states or to determine the proportion of dissolve volatiles in a glass, it is preferable to normalize to the full area of the spectra after application of the temperature correction (Le Losq et al. 2012). The baseline correction to investigate volatiles in glass is reported in detail in Le Losq et al. (2012).

3.8 Size of the sampled area

Raman spectrometry is an additive spectroscopy technique Each component (crystal, glass, gas) will contribute with its characteristic signal. It is therefore particularly important before doing any Raman analysis to observe the object to be analyzed. For example, if the object consists of two-phases, it will be necessary to focus the laser beam only on one of them, otherwise, being an additive method, the resulting spectrum will be a convolution of the distinct signals of the two phases. This could appear obvious, but in the literature, more and more articles propose corrective terms depending on the opening of the confocal hole, the nanoparticle size, and so on, most of which have no physical meaning.

An example of the importance of the sampled area size is represented by the analysis of a very well know feature in volcanology studies: the fluid inclusions. Fluid inclusions are memories of parental liquid state trapped in a crystal during magma evolution, and by investigating fluid inclusions, volcanologist can decipher the history of a volcanic eruption (Nasdala et al. 2003; Metrich et al. 2011). Since a fluid inclusion consists of a glass phase incorporated inside a crystal, to obtain good Raman spectra, a confocal system is needed. Nevertheless, the Raman spectra often will provide the sum of the signals related to the crystal and to the glass. In this case, the Raman spectrum of the inclusion can be easily obtained by subtracting the spectrum of the mineral host to the raw spectrum (Figure 8). Similar investigation can be made for nanoparticules dissolved in glass.

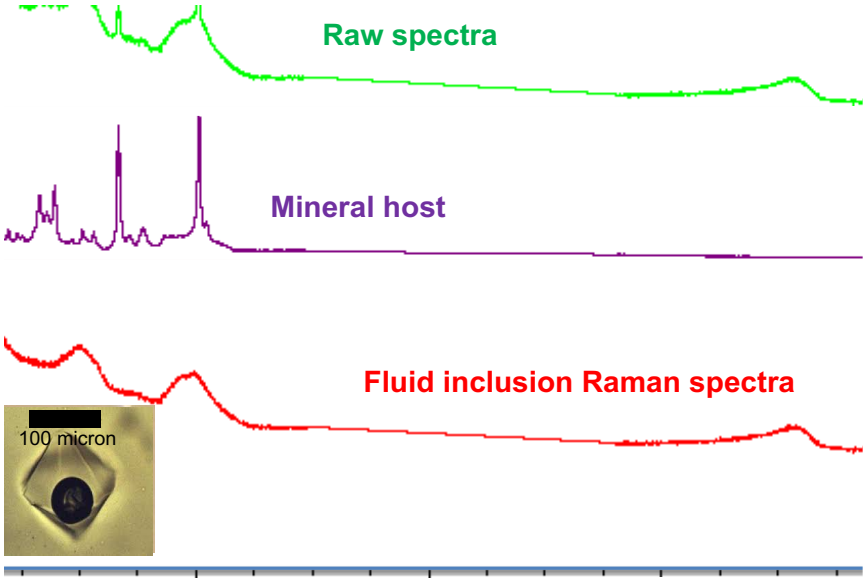

Figure 8: Raman spectra of diphasic samples, which can be decomposed in 2 signals, one associated to the glass phase, and the other one to the surrounding crystal.

4. Other types of Raman spectroscopy

4.1 Hyper-Raman Scattering (HRS)

HRS was developed by Denisov et al., (1984, 1987) and corresponds to a non-linear spectroscopy where two incident photons (ω_i) produce one scattered photon (ω_s) after interaction with an excitation (ω_p) in the medium. Infrared (IR)-active modes are seen in Hyper-Raman Spectroscopy, HRS, but there are *HRS*-active modes that are silent both in Raman scattering and IR, while acoustic modes are *HRS* forbidden. As the *HRS* signals are usually very weak (typically 10^6 times smaller than Raman scattering), early work was limited in resolution, and the results did not include the low frequency region. Currently, technical advances in pulsed laser sources and charge coupled devices (CCD) allow one to reach resolutions comparable to that of Raman spectroscopy with reasonable acquisition times. HRS gives complementary information to Raman scattering and, in particular on glasses where all vibration modes are not active in the IR or RS (Helhen et al., 2000, 2002, Simon et al., 2006, 2008).

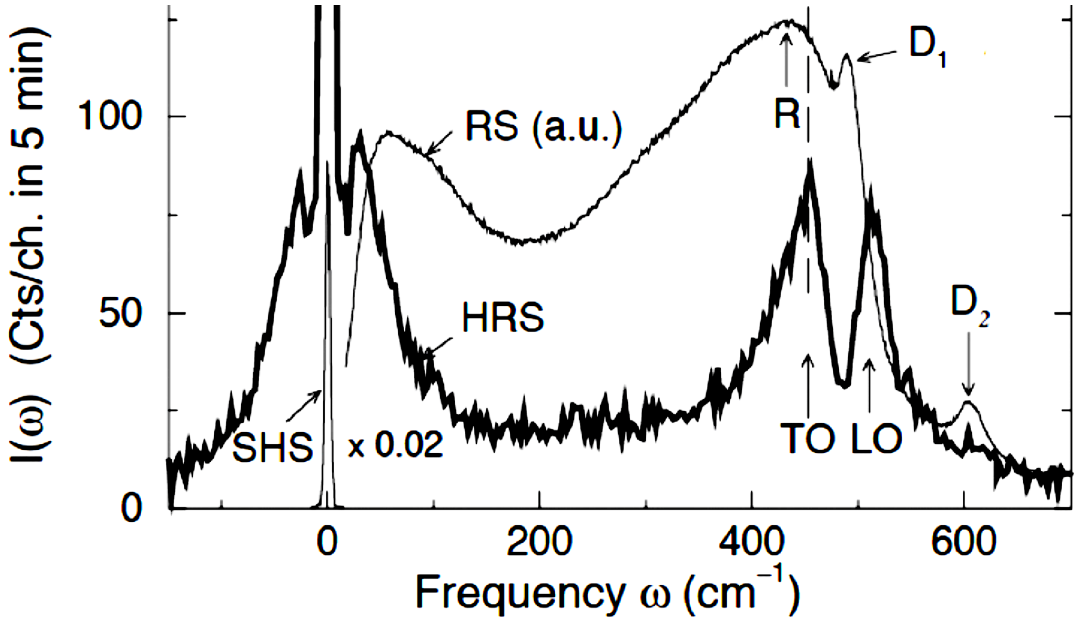

Figure 9: Raman and Hyper-Raman spectra of silica (modified after Helhen et al., 2000) where ω is the wavenumber.

Figure 9 show:

- i) RS, Raman spectrum obtained with a T64000 Jobin-Yvon® a triple spectrometer operating at 514.5 nm with a CCD camera,
- ii) HRS, hyper-Raman spectrum of silica at low frequency after standard treatment, with frequencies in wavenumbers ($\omega/2\pi c$).

Figure 9 clearly shows that the Hyper-Raman Spectrum of silica contains more vibrational information than the classic Raman spectrum. However, HRS measurements are more difficult to register than classic RS and actually, this new technique is essentially used only by physicists to investigate simple glass system, like SiO_2, B_2O_3, or some binary glasses. Also, this technique brings very important information on the low frequency vibrations in amorphous system. This technique is probably very powerful tool to investigate amorphous materials but needs to be more used and adapted for at high pressure or high temperature studies.

4.2 Surface Enhanced Raman Scattering (SERS)

SERS is a phenomenon in which the Raman scattering intensity from molecules close to the surface of certain finely divided metals is enhanced by a factor of about 10^6. Raman spectra arise from the vibrational frequencies of the molecules and provide molecular information that is particularly valuable in nano-chemistry. The inherently low sensitivity of conventional Raman scattering limits its applicability, but sensitivity enhancement by SERS has resulted in more widespread applications, especially in surface chemistry where the environmental sensitivity of vibrational spectra reveals how molecules interact with surfaces.

The first paper reporting the phenomenon was published by Fleischmann et al. (1974), who observed a potential-dependent Raman signals from pyridine adsorbed on a silver electrode that had been electrochemically roughened in potassium chloride aqueous electrolyte. Two groups (Jeanmaire and Van Duyne, 1977; Albrecht and Creighton, 1977) clarified the degree of Raman signal enhancement in the pyridine-on-silver system and proposed enhancement mechanisms based on electromagnetic and chemical effects, respectively. Van Duyne proposed the SERS acronym and claims that his group discovered SERS. The initial paper of Fleischmann et al. (1974) has been cited more than 1200 times, and SERS is now very well used in the chemical sciences.

The main contributor to the intensity enhancement is an electromagnetic effect arising from the laser excitation of localized surface plasmons (collective electron oscillations) at rough metal surfaces, which creates an enhanced electric field. Both the incident and scattered light are influenced by this field enhancement, resulting in a total Raman signal enhancement proportional to the energy field. A smaller contribution to SERS enhancements comes from a charge transfer mechanism for adsorbed molecules with appropriate acceptor or donor orbitals that interact with the metal substrate. The metals exhibiting the largest SERS enhancements are silver, gold and copper. More details on SERS and its applications are given by Fleischmann et al. (1974) and Jeanmaire and Van Duyne, (1977).

Since 1980 SERS has been widely developed for the investigation of biological interactions, or to determine some biological units in organisms. However, this technique can be also useful in both materials and earth sciences to enhance the Raman signal obtained with a portable Raman spectrometer. By using and developing the SERS it is probably possible to realize direct in situ analyses directly when doing earth science exploration (volcanology, mineral exploration). Moreover, as done for biology researches, SERS can be used in earth and mineral sciences to enhance the Raman signal, in particular to analyze dissolved gases in glasses, and melts. Ergo, perhaps it would be possible using SERS to increase the sensibility and determine dissolved water, and CO_2 concentration. Recently, Haidar et al. (2015) have shown that by using Silver-Gold nanoparticules, it is possible to enhance a Raman signal. This can open some new ways to developpe in situ Raman spectroscopy with portable Raman spectrometers.

5. Chemical effect on Raman spectra of glasses

In this section, we present the main glasses used in fiber technology, namely SiO_2, GeO_2, and some silicate glasses. Readers interested by borosilicate, aluminate can see the extensive review of the chemical effect on glass available in Neuville et al. (2014). We can mention that Raman spectroscopy is a fantastic tool to investigate aluminosilicate glasses (Matson et al., 1983, McMillan, 1984, 1985, McMillan and Piriou, 1982, 1983, McMillan et al., 1992, Mysen 1999, 2003, Mysen and Frantz 1992, 1993, 1994a,b, Neuville et al., 2004, 2006, 2008, 2010, Licheron et al., 2010, Le Losq and Neuville, 2013, Kojitani et al., 2013, Le Losq et al., 2014, 2017, 2019), borate and borosilicate glasses (Chryssikos et al., 1990, Katmisos et al., 1987 ; Akagi et al., 2001, Maniu et al., 2003, Yano et al., 2003a,b, Lenoir et al., 2008, Manara et al., 2009a,b, Meera and Ramakrishna, 1993), iron silicate glasses (Mysen et al., 1980a, 1985a,b, Magnien et al., 2004, 2006; Roskosz et al., 2008, Cochain et al., 2012, 2013) and titanosilicate glasses (Henderson and Fleet, 1995, Mysen and Neuville 1995).

5.1 SiO_2 polymorphs

Normalized Raman spectra of metallic silicon (Si), silica polymorphs and amorphous SiO_2 (glass) are showed in Figure 10. The first-order Raman spectrum yields energies for the $k = 0$ optical modes of 520.2 ± 0.5 cm^{-1} for Si (k = wavevector of the mode). Metallic Si has a diamond structure with space group *Fd3m* with two atoms in the smallest volume unit cell. It has one triply degenerated optic mode at $k = 0$ with symmetry F_{2g}, Raman active, but infrared inactive. The optical mode producing the line at 520 cm^{-1} is not polar, thus, it is not affected by transverse optical (TO) or longitudinal optical (LO) mode splitting, and a single Raman line is observed. A weak second order transition is also present around 970 cm^{-1}. The ratio of the peak intensity of the second-order band to that of the first-order line is found experimentally to be ~$3x10^{-3}$, even if the relative intensity of these two peaks depends strongly on the crystallinity and local organization of the Si (Kravets and Kolmykova, 2005).

Among the silica polymorphs (same chemical composition, but different crystal structure) quartz is the most common one. In Figure 9, the Raman spectrum of α-Quartz, shows a very strong vibration at 466 cm^{-1}, lower than the 520cm^{-1} observed for metallic Si, which corresponds to A_1 Raman active mode. The A_2 (IR-active) and the E modes are split into longitudinal (LO) and transverse optic (TO) modes.

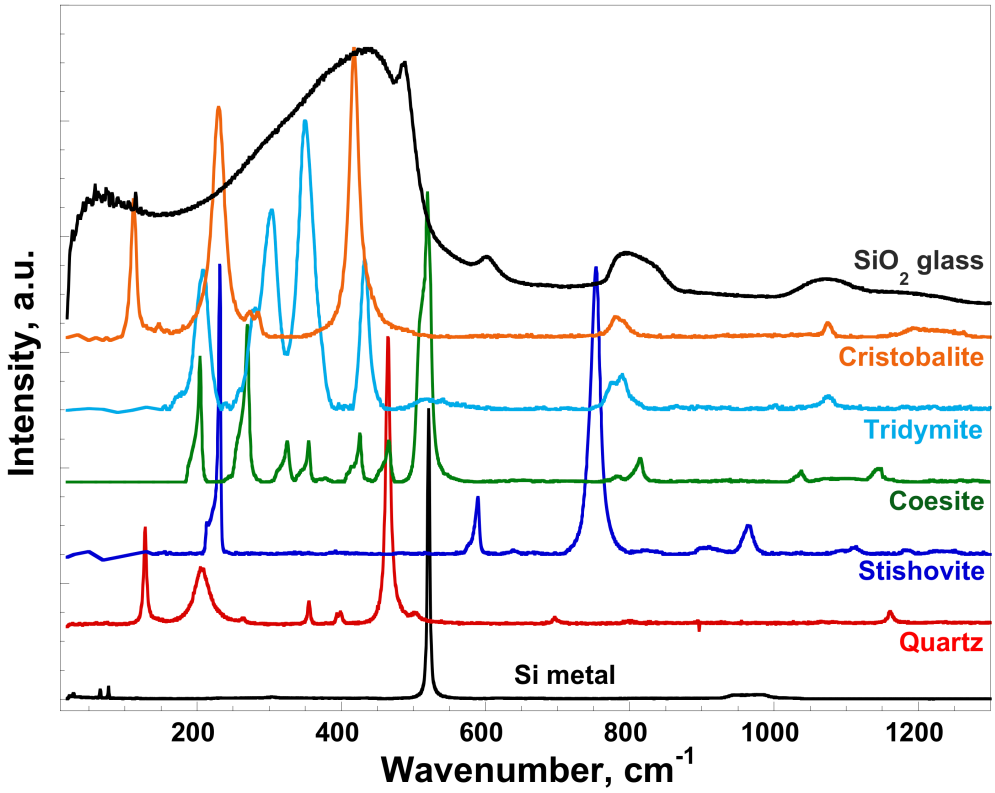

Figure 10: Raman spectra of metallic Si, SiO_2 polymorphs and amorphous SiO_2.

To a first approximation, we can explain the lower frequency observed for SiO_2 compared to Si by the fact that the SiO_2 molecule is heavier than Si (heavier atoms will have corresponding vibrational bands at lower wavenumbers because of their higher mass and its effect on the vibrational frequency). Crystalline SiO_2 has been studied extensively with both the early mercury arc lamp source and more modern laser excitation. One of the first reviews of optical lattice vibrations in quartz and their assignments was made by Scott and Porto (1967), subsequently She et al. (1971) reported more accurate measurements of Raman intensities in quartz and Bates and

Quist (1972) and Etchepare et al. (1974) obtained the polarized Raman spectra of α-quartz. The lattice dynamics of quartz have also been calculated by many authors (Saskena et al. 1940; Kleinman and Spitzer, 1962, Etchepare et al. 1974). In the figure 9, we present only α-quartz but the lattice structure of α- and β- quartz are very similar; the β-phase appears at temperatures higher than 900 K (Bates et Quist, 1972).

Most of silica polymorphs (quartz, trydimite, cristobalite, coesite) consist of SiO_4 tetrahedra linking together by corners. Stishovite is the exception, since in this high-pressure polymorph the Si atoms are octahedrally coordinated. A comprehensive review of the Raman active vibrations, of the SiO_2 polymorphs can be found in different papers (Sharma et al. 1981; Hemley et al. 1986; Kingma and Hemley 1994; McMillan et al. 1994). It is clear that Raman spectroscopy is a powerful tool for investigating and identifying crystalline polymorphs as well as for investigating the structure of amorphous phases such as glasses and liquids. For example, nowadays, Raman spectroscopy is commonly used to characterize materials in online industrial processes for "quality control" for identification of different mineral phases using Raman spectral databases (like RRUFF, www.rruff.org) and organic compounds in industrial processes.

The Raman spectrum of the SiO_2 glass shows much broader vibrational bands with respect to the crystalline SiO_2 polymorphs, reflecting its amorphous nature. The broad band centred at ~ 435 cm^{-1} corresponds to the symmetrical Si–O–Si stretching mode, whereas the two well pronounced features at 490 and 600 cm^{-1}, also called defect lines D_1 and D_2, are associated to the breathing modes of 4-membered and 3-membered rings, respectively. In the high frequency region, there are only two weak bands which are associated to Si-O asymmetric stretching motions in the tetrahedral units.

5.2 SiO_2 versus GeO_2

Bulk composition change

Glass fiber are mainly based on two oxides, SiO_2 and GeO_2, and a few other components that are added in order to improve the desired optical and/or thermo-mechanical properties. Among glasses, silica (SiO_2) is the most used material in fiber optics (particularly for optical fiber telecommunications), because it has many favorable properties, such as the extremely low propagation losses and the mechanical resistance provided. In optical fiber technology, in order to vary the glass refractive index, and also to enhance the solubility of Rare Earth Elements in the fiber core, a doping with several elements is carried out, with the most common ones being GeO_2, Al_2O_3, P_2O_5. Therefore, in this section, we are going to show, first of all, the evolution of the Raman spectra of mixing $(Ge_XSi_{100-X})O_2$ glasses, and one glass Ge95Al which correspond to 95% GeO_2 and 5% Al_2O_3 in mole (Figure 11) and secondly, to discuss the modifications occurring in the SiO_2 glass network upon addition of a few mol% of Al_2O_3 (Figure 12).

The Raman spectra of GeO_2 glass along with those of the binary glasses and SiO_2 are shown in figure 11. The band assignments for GeO_2 glass are similar to those of SiO_2 glass, even if the bands are shifted to lower wavenumber because of the larger mass of Ge relative to Si. Band assignments for GeO_2 are based on earlier studies, e.g. Henderson et al. (2009); Henderson and Fleet, (1991) and Micoulaut et al., (2006). The strongest band in GeO_2 glasses at ~ 420 cm^{-1} is associated to the symmetric stretching modes of the Ge–O–Ge bridging oxygens. The width of this band is much narrower compared to the equivalent symmetric stretching modes of amorphous SiO_2. This difference has been ascribed to a narrow distribution of Ge–O–Ge intertetrahedral angles for GeO_2 glass compared to the SiO_2 ones, based on Raman, neutron and x-ray diffraction data (Micoulaut et al., 2006). At ~ 520 cm^{-1}, the evident feature is the D_2 '*defect*' band, and analogously to the SiO_2 glass described above, it is associated to the breathing mode of 3-membered GeO_4 tetrahedra rings.

Micoulaut et al. (2006) recognized that the D_2 in GeO_2 glass has a higher relative intensity with respect the main band, in comparison with the corresponding breading mode of SiO_2 glass, suggesting that GeO_2 glass network is built on a larger proportion of three-membered tetrahedra rings. The broad contribution between 550 and 650 cm^{-1} derives from Ge–O–Ge bending modes, which are split into transverse optical TO (556 cm^{-1}) and longitudinal optical LO (595 cm^{-1}) modes, associated with Ge and O motion (Galeener and Lucovsky, 1976; Micoulaut et al. 2006).

In the high frequency region, the two bands at ~ 860 and 988 cm^{-1} are related to the asymmetric stretching bands of the bridging oxygens (Ge–O–Ge), and respectively associated to transverse optical (TO) and longitudinal optical (LO) split modes.

In addition, in the very low frequency region, there is a peak at ~60 cm^{-1} which is the so-called boson peak (Malinovsky and Sokolov, 1986; Buchenau et al., 1986). This peak has been ascribed to excitations associated with rotational motions of almost rigid tetrahedra (Buchenau et al., 1986; Helhen et al., 2000, 2002). Helhen et al. (2002) considered that this peak, observed for different silicate glasses, increases in intensity and shifts to higher frequency with higher distortion of the SiO_4 tetrahedra. In our case, the boson peak shift to lower frequency with the Si/Ge substitution and toward higher frequency with Ge/Al substitution (Figure 10).

Glasses along the $(Ge_XSi_{100-X})O_2$ join have been studied previously both at room and at high temperatures using Raman spectroscopy (Shibata et al., 1981; Sharma et al., 1984; Nian et al., 1989; Duverger et al. 1998; Martinez et al., 2003; Majerus et al., 2008; Henderson et al., 2009). At high GeO_2 contents the spectra resemble that of pure GeO_2 while at high SiO_2 contents they resemble that of pure SiO_2. With increasing SiO_2 contents the small feature of GeO_2 at ~ 340 cm^{-1} is lost, the symmetric stretching band at ~420 cm^{-1} begins to move to higher frequencies and broaden. The asymmetric stretching bands TO/LO, in the high frequency region, also change with the LO (988 cm^{-1}) component being lost and the TO (860 cm^{-1}) band moving toward higher values and decreasing in intensity. All glasses containing Ge do not have the transverse optical mode of SiO_2 at ~1055 cm^{-1}. The Ge-O-Ge bending modes in the 550-650 cm^{-1} region broaden slightly, move to higher wavenumbers and decrease in intensity. In the mixed glasses GeO_2-SiO_2, new contributions, associated to Ge-O-Si vibrational modes, are observed at ~683 cm^{-1}, ~1000 cm^{-1} and ~1100 cm^{-1}. The band at ~1000 cm^{-1} is due to Ge-O-Si asymmetric stretching while the 683 cm^{-1} band is due to Ge-O-Si bending modes and the 1100 cm^{-1} band is due to asymmetric stretching of Si-O-Si bonds which are not split into TO/LO components as a result of increase disorder in the mixed glasses (cf., Sharma et al., 1994; Majerus et al., 2008; Henderson et al., 2009). The Si-O-Si bending modes in the 750-850 cm^{-1} region begin to appear after 50 mol% SiO_2. The D_1 and D_2 "defect" bands of SiO_2 are not observed in any of the mixed composition glasses and the intensity of the Ge-O-Si bending modes at ~783 cm^{-1} increase in intensity with increasing SiO_2 (cf., Henderson et al., 2009).

Studies on $(Ge_XSi_{100-X})O_2$ glasses done at high temperature, have shown that glasses that have been annealed or glasses heated to high fictive temperatures then quenched, present a shift in the ~440 cm^{-1} band to higher wavenumbers and broadening of the D_1 and D_2 SiO_2 bands. Therefore, structural variations between quenched/annealed glasses and glasses at high temperatures should occur, with quenched glasses having i) the average T-O-T (where T = Ge or Si) angle narrows and ii) larger proportions of 3- and 4-membered rings of SiO_4 or GeO_4 tetrahedra (Martinez et al., 2003; Henderson et al., 2009).

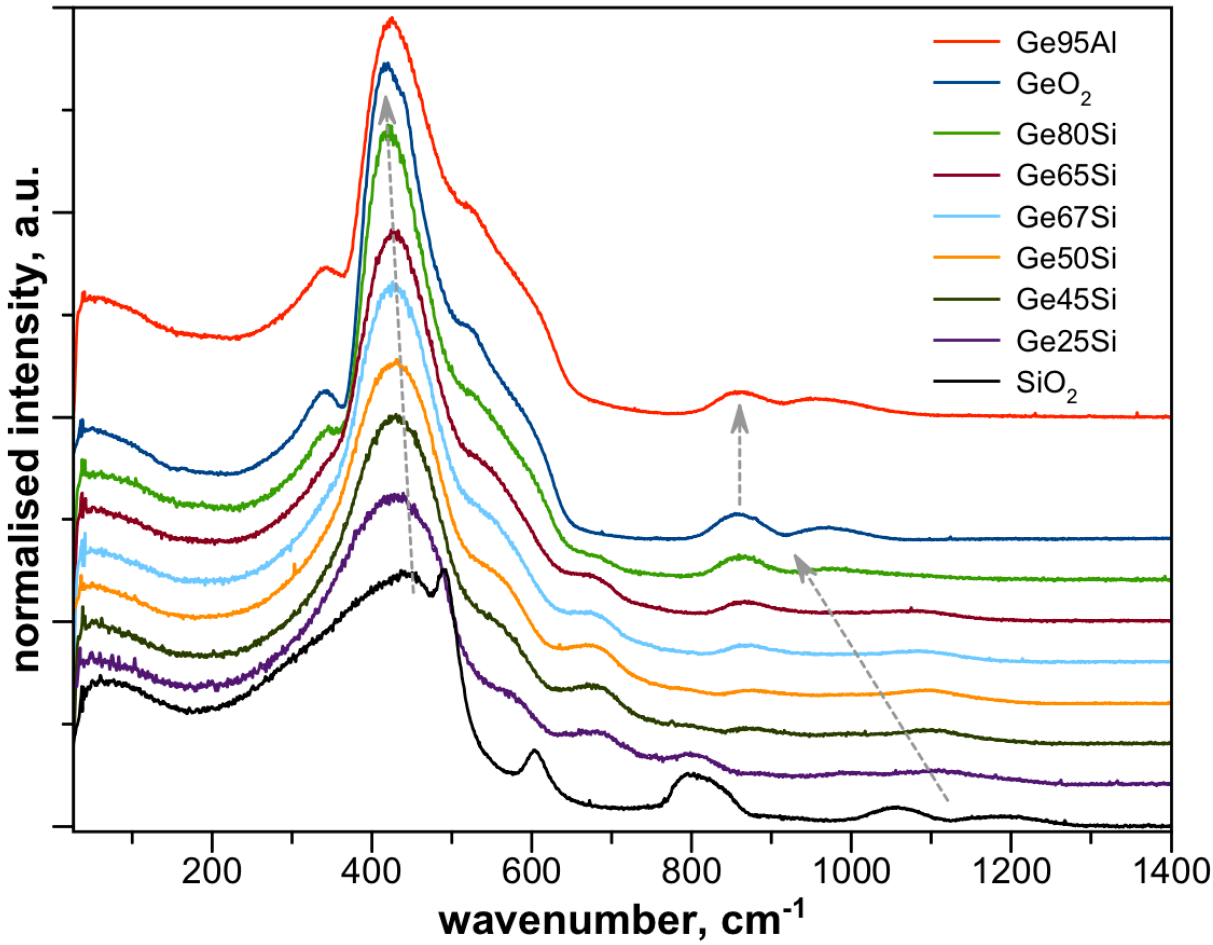

Figure 11: Raman spectra of SiO_2-GeO_2 glasses and Ge95Al.

In the case of the Ge95Al, (95%GeO_2 and 5%Al_2O_3 in mole%), the peak at 440 cm^{-1} shifts to high frequency and decreases in intensity. Moreover, the broad contribution between 550 and 650 cm^{-1} shifts toward higher wavenumbers, and the band at ~ 990 cm^{-1}, associated to LO asymmetric stretching of bridging oxygens, markedly increases in intensity. These changes can be attributed to the presence of Al in four-fold coordination within the germanate glass network. It is well known that in some calcium aluminate glasses the band at ~600 cm^{-1} can be assigned to transverse motions of the bridging Al-O-Al linkages (McMillan and Piriou, 1983; Neuville et al., 2010), while the higher frequency 780 cm^{-1} band can be assigned to symmetric stretching of AlO_4^- units in the glass. Thus, Al entering the tetrahedral sites could be responsible for the shift of the 440 cm^{-1} band to higher frequency, and of the shift of the shoulder at ~600 cm^{-1} and a decrease in intensity and a small shift to low frequency observed for the 880cm^{-1} bands.

Application in a glass fiber

Single mode optical fibers can be briefly described as cylinder with a small central portion, in the order of 8 μm (fiber core), surrounded by another glass with a lower refractive index (cladding). Usually a few mol% of Al_2O_3 (or GeO_2) are added to the SiO_2 core to increase its refractive index, and to further enhance the incorporation of other dopants. Figure 12 shows the Raman spectra of the doped core and of the cladding of a silica fiber preform. The surrounding cladding is almost exclusively composed by SiO_2 (99.8mol%) and the spectrum resembles the spectrum of pure SiO_2, with the well pronounced D_1 and D_2 "defect" lines in the low frequency region, and the relatively

less intense vibrational features above 950 cm^{-1}. In the core, the presence of ~1.5mol% Al_2O_3 induces several variations in the Raman spectrum, and in turn, in the glass network. The modifications observed in the low frequency region (Figure 12) can be ascribed to variations of the Si–O–Si intertetrahedral angle, and in particular, the variations in the relative intensities of the D_1 and D_2 lines suggest that Al modifies slightly the rings statistic distribution. In the high frequency domain, the cladding presents two well-separated peaks, whereas the core has a much broader contribution. The curve-fitting analysis of the 960-1300cm^{-1} frequency region highlights the modification of the high frequency regions, and in particular, the broadening and the shift toward lower frequency of the 1150cm^{-1} band (Figure 12). Cicconi et al. (2017) reported that the shift of this band, after Al introduction, is associate to Al^{3+} entering the tetrahedral site causing an increase of the average T-O bond length.

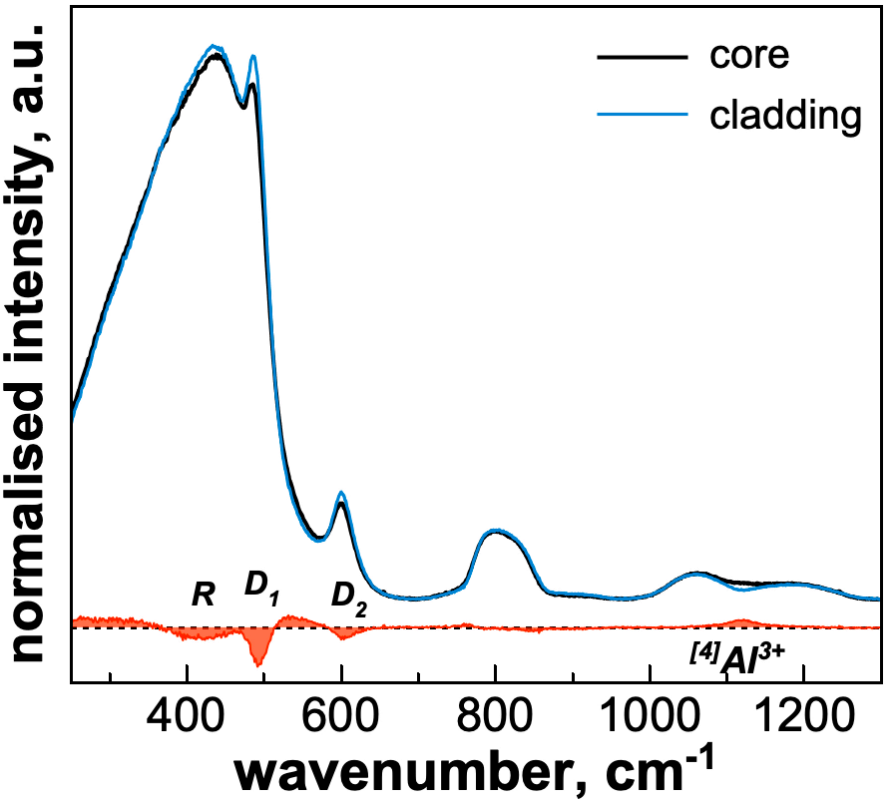

Figure 12 – Raman spectra of a silica fiber preform, in the cladding and in the Al-doped core. In orange, the difference between both spectra.

5.3 Amorphous silicate glasses

Raman spectra on amorphous materials were first made by Raman and Krishnan (1929) (see figure 4) and just after Raman, Hollaender and Williams (1929, 1931) investigated several glasses and in particular an ordinary plate glass, which corresponds to a soda-lime silicate glass (window glass). In the Raman spectrum of the plate glass, they identified 11 bands similar to those observed in the IR spectrum of fused quartz by Reinkober (1911). Their spectra clearly showed that the number, intensity and position of bands in amorphous quartz is slightly different to the bands observed in the different polymorphs of quartz. Thus, Hollaender and Williams (1929, 1931), by using Raman spectroscopy, were the first to observe the differences between crystals and glasses, just a few years before Warren (1934a,b) and Zachariasen (1932).

Among the vibrations observed by Hollaender and Williams (1929, 1931), there was a new band appearing at very low frequencies, the Boson Peak, BP, located near 80 cm^{-1}, and this band is considered to be a Raman signature of tetrahedrally connected glasses. It has been ascribed to

Raman scattering involving rotational motions of almost rigid tetrahedra (Buchenau et al. 1986) although its origin remains controversial and is a continuing area of interest in condensed matter physics. In the case of silica glasses, the intensity of the Boson peak increases and the position shifts to higher frequency with increasing distortion of the SiO_4 tetrahedra (Hehlen et al. 2000, 2002; Neuville 2006). This is clearly visible in Figure 13 for SiO_2 glass and for glasses in the binary system Na_2O-SiO_2 (soda silicate glasses Na1, Na12, Na25, Na33, Na40) where the BP shift from 54 up to 70 cm^{-1} between 0 and 40 mole % Na_2O. Also in the Figure 13, different behavior of the Boson peak is clearly visible, as a function of the element. Light elements (Li, Na, Mg, Ca) produce a shift to higher frequency with the increase of their amount content whereas heavy elements (like K and Ba,Sr (Novikov et al., 2017) and Cs (O'Shaughnessy et al., 2017)) do not modify the frequency of the BP which stay almost constant at low frequency around 50 cm^{-1} like in silica glass. These differences are probably due to differences in Raman cross sections and channel effect.

In figure 13 are reported Raman spectra of several silicate glasses in the binary systems Li_2O-SiO_2, Na_2O-SiO_2, K_2O-SiO_2, MgO-SiO_2, CaO-SiO_2, BaO-SiO_2. The spectra are labelled according to the molar content of alkali/alkali-earth oxides (i.e. Na40, represents a glass with 60mol% SiO_2 and 40mol% Na_2O). Depending on the kind of element, and on its molar content, the Raman spectra strongly change. In particular, the Raman bands in the low frequency region (250-650cm^{-1}), associated to the symmetric stretching modes of the Si–O–Si bridging oxygens, move to higher frequencies with addition of alkali/alkali-earth elements. In the high frequency region, SiO_2 has two weak bands associated to asymmetric stretching motions, but the insertion of network modifiers strongly enhances the intensity of these bands. Higher amounts of alkali/alkali-earth elements produce the whole band to shift to lower frequencies because of the increasing amount of non-bridging oxygens (NBO), and the magnitude of the shift, for a constant amount of alkali/alkali-earth element introduced, will depend on the type of cation (e.g. Li > Na > K, Fig. 13).

Worth to be noted, in Figure 13, is that the introduction of 1 mol% of sodium does not produce strong changes in the Raman spectra of silica glass. Also, it is clearly visible that introduction of around 1% of network modifier like Na produces some small Q^3 species but not really visible in the Na1 spectra, and not really affect the ring distribution as produce by adding 1% Al_2O_3 (see Figure 12).

In the figure 13, four frequency domains are visible: the very low frequency part (Boson peak) between 15 and 200cm^{-1} (see discussion below), the low frequency between 200 and 800 cm^{-1}, the intermediate between 700 and 900 cm^{-1} only visible for high silica content (SiO_2 >60% mole) and the high frequency domain, 900-1250cm^{-1} which correspond to the Si-O stretching vibrations resulting from the different Q^n species.

The low-frequency domain - 200-800cm^{-1}, the room-temperature Raman spectra exhibit a strong band centered near 500 cm^{-1} for SiO_2 glass with a shoulder near 450 cm^{-1}, and another band near 600 cm^{-1} similar to other published spectra of vitreous silica (Bell et al. 1968; Bell and Dean, 1972; Seifert et al. 1982; Phillips, 1984; Galeener et al., 1984; McMillan et al. 1994). Bands near 400-600 cm^{-1} in silicate networks are usually the result of vibrations of the bridging oxygens associated with 3-, 4-, 5-, 6- or higher-membered rings of tetrahedra (Sharma et al. 1981; McMillan and Piriou, 1982; Galeener, 1982a,b; Mysen et al. 1980a; Seifert et al. 1982; Galeener et al. 1983; Sharma et al. 1985; McMillan et al. 1994; Pasquerello and Car, 1998; Pasquarello, 2001; Umari and Pasquarello, 2002; Umari et al. 2003; Rahmani et al. 2003). In SiO_2 glass, three peaks near 440 cm^{-1}, 495 cm^{-1} and 606 cm^{-1} are visible and the first peak is ascribed to the predominant motions of oxygen atoms, involved in Si-O-Si bonds in five-, six or higher-membered rings (Sharma et al. 1981; McMillan et al. 1994; Kalampounias et al. 2006). The second band, near 485-490 cm^{-1}, is usually called the D1 band and is formed by breathing motions of oxygen atoms (i.e. movements of oxygen perpendicular to the Si-O-Si plane) in regular, but slightly puckered, four-

membered rings (Sharma et al. 1981; Galeener, 1982b; Pasquarello and Car, 1998; Umari and Pasquarello, 2002; Umari et al. 2003; Rahmani et al. 2003). The third band, located near 606 cm-1, is called the D2 band and is ascribed to the breathing motion of oxygen atoms in planar three-membered rings (Galeener, 1982a,b; Galeener et al. 1983; Pasquarello and Car, 1998; Umari and Pasquarello, 2002; Umari et al. 2003; Rahmani et al. 2003). Note that the exact nature of the vibration, i.e stretching or bending for instance, seems to be uncertain but all studies point out the motion of oxygen in Si-O-Si linkages (McMillan et al. 1994).

With addition of alkali or alkaline earth elements these bands evolve from a peak around 500 cm^{-1} and a shoulder at 600 cm^{-1} for M20 (M=Li, Na, K) up to a peak at 660 cm^{-1} and its shoulder at 730 cm^{-1} for Mg62. The peak at 500 cm^{-1} has been assigned to Si-O^0 rocking motions in fully polymerized SiO_2 (Q^4) units (Bell and Dean, 1972; Phillips, 1984) while the maximum at 600 cm^{-1} has been assigned to Si-O-Si bending motions in depolymerized structural units (Lazarev, 1972; Furukawa et al. 1981). In all case, contrarily to the general idea, it is clearly visible that this frequency region evolves a lot as a function of the network modifier element. Light elements produce almost similar change and their evolutions show always an increase of the frequency with increasing their amount content. But in the case of heavy element like K or Cs (O'Shaughnessy et al., 2017), intense D1 and D2 bands are still visible for more than 30% of SiO_2. The different behavior between light and heavy elements on the Raman spectra of silicate may be produced by some percolation channel enhanced by heavy element like K or Cs.

The intermediate frequency region - 700-850 cm^{-1}; in the case of SiO_2, the 800 cm^{-1} band is attributed to Si-O stretching involving oxygen motions in the Si-O-Si plane (McMillan et al. 1994) or to the motion of the Si atom in its oxygen cage (Mysen et al. 1982). Another attribution arises from the central force model of Sen and Thorpe (1977), which links the 800 cm^{-1} band to the threefold –degenerate "rigid cage" vibrational mode of TO_2 units (Galeener, 1979). This peak shifts slowly to higher frequency and decreases in intensity with MO up to its disappearance. It is also asymmetric and has been assigned to two bands with TO/LO splitting (Galeener and Lucovsky, 1976; Galeener et al. 1983).

The high frequency region - 850-1300 cm^{-1}; Si-O stretching is responsible for the broad band observed near 1100 cm^{-1} (Bell et al. 1968; Sen and Thorpe, 1977). Several studies have noted that different peaks are convoluted in this band and arise from the T-O stretching in different Q^n tetrahedral units (see McMillan (1984) and Mysen (2003) and references therein). The intensity of these bands increases with alkali or alkaline-earth content, and by curve fitting (spectral deconvolution) of this high frequency region, three Gaussian bands can be observed at 1000, 1100 and 1200 cm^{-1} in silicate glasses. Most of the time, deconvolution of this area were made by using several gaussian bands (Mysen et al. 1982; Seifert et al. 1982; McMillan, 1984; Neuville and Mysen, 1996; Fukumi et al., 1990; Neuville et al. 2004, 2006, 2008; Le Losq and Neuville, 2013, Le Losq et al., 2014, 2017) but recently some papers shown that it is also possible to made deconvolution of this large frequency domain by using Lorentzian bands (McMillan, 1984; Zotov, 2001; Bancroft et al., 2018, Nesbitt et al., 2018, 2019 and reference therein). For example, Bancroft, Nesbitt and coworkers proposed to use several Lorentzian bands for the same Q species (called Q^n-*m*, *n* is the number of bridging oxygen and *m*, the number of bands for the Q^n species) and from these bands they succeeded to calculate the Q species concentration and find some good agreement with those obtained by NMR spectroscopy (Nesbitt et al., 2019). This deconvolution technique is quite robust, but it requires several assumptions and also to already have NMR and XPS spectroscopies data, also another problem of this treatment is that the proportion of Lorentzian band in each band Q^n-*m* varies randomly. Finally, the proportion of the Q species is a

sum of the Q^n-m which also required as assumption that Raman cross-section of Q^n-m are the same. This new-treatment with Lorentzian band can be very attractive and can bring important thermodynamics information's but are still in progress.

We assumed that classic treatment using Gaussian band is actually the most accurate and easy way to use for Raman non-expert. Bands expressed in this high frequency domain arise only from the expression of particular vibrational modes of the TO_4 tetrahedra (Le Losq and Neuville, 2013). For pure SiO_2 glass there are only two peaks, one near 1050 cm^{-1} and a wider peak centered near 1200 cm^{-1}. These two peaks (Figure 13) are also visible in the Na1 Raman spectra (MX = (100-X)%SiO_2-XMO with M= Li_2, Na_2, K_2, Mg, Ca, Ba), and with increasing Na_2O content (Na12= NS7 glass), the intensity of the peak at 1050 cm^{-1} increases strongly. We can note, that in the case of silica glass, the high frequency part near 1200cm^{-1} can be split into two bands using deconvolution (Seifert et al. 1982, Neuville and Mysen, 1996), named $Q^{4,II}$ (1100 cm^{-1}) and $Q^{4,I}$ (1170 cm^{-1}), to account for the Q^4 signal in all spectra although these assignments remain controversial. According to the Sen and Thorpe (1977) model, the $Q^{4,II}$ band represents vibrations associated with BOs with lower T-O-T angles than the $Q^{4,I}$ band. With increasing MO content, the $Q^{4,I}$ (1170 cm^{-1}) band is lost and new bands appear at lower frequencies for NBO vibrations associated with Q^3, Q^2, Q^1 and Q^0 tetrahedra. The bands shift to lower frequency as a function of increasing MO and in the case of the Na20 glass spectra, the 960 cm^{-1} band is assigned to $Si\text{-}O^-$ stretching in Q^2 species (Brawer and White, 1975; Mysen et al. 1982; Seifert et al. 1982; McMillan, 1984; Mysen, 1999). The 1100 cm^{-1} band is ascribed to $Si\text{-}O^-$ stretching occurring in Q^3 units (Brawer and White, 1975; Virgo et al. 1980; McMillan, 1984). In the Na20 Raman spectrum, one can account for Q^4 vibrations using one band, located near 1150 cm^{-1} (see for instance Mysen, 2003).

In Figure 13, it is clearly visible that Raman spectra change a lot as a function of silica content, and also at the same silica content as a function of alkali or earth-alkaline elements, as can be observed for Li20, Na20 and K20. The high frequency area between 800 and 1200 cm^{-1} change a little in term of Q species distribution, and these changes are very well described by Mysen and Frantz (1992, 1993, 1994). But also, important changes are obvious at low frequency between 400 and 600 cm^{-1}, where the size of the alkali element affect the ring statistic distribution, in particular asthe ratio z/r decreases, D1 and D2 bands are more visible and play important role in the structure of the glass. This has been demonstrated recently by Le Losq et al. (2017) which proposed an "Universal idea for the glass structure" composed by channel percolation in all sort of silicate glasses. In the case of alkali element, the cation size affects the rings statistic distribution up to more than 40%, which is visible in the Raman spectra of Cs silicate (O'Shaughnessy et al., 2017) for alkaline-earth element this effect is only visible up to 33% of barium (Figure 13, Ba33).

The high frequency envelope decreases in frequency with decreasing SiO_2 content which is correlated to the change in Q distribution from Q^4 for silica glass to Q^0 species for orthosilicate glass (33% of SiO_2). Figure 13 also shows the Raman spectra for depolymerized glasses with high MO content. In this case the intensity maximum of the T-O-T stretching bands shows clearly Si in Q^0 and Q^1 species like for the Mg62 and Mg56 Raman spectra. These changes visible between 100 and 37% of alkali or alkaline earth element are similar at those produced by lead in silica glasses (Ben Kacem et al., 2017).

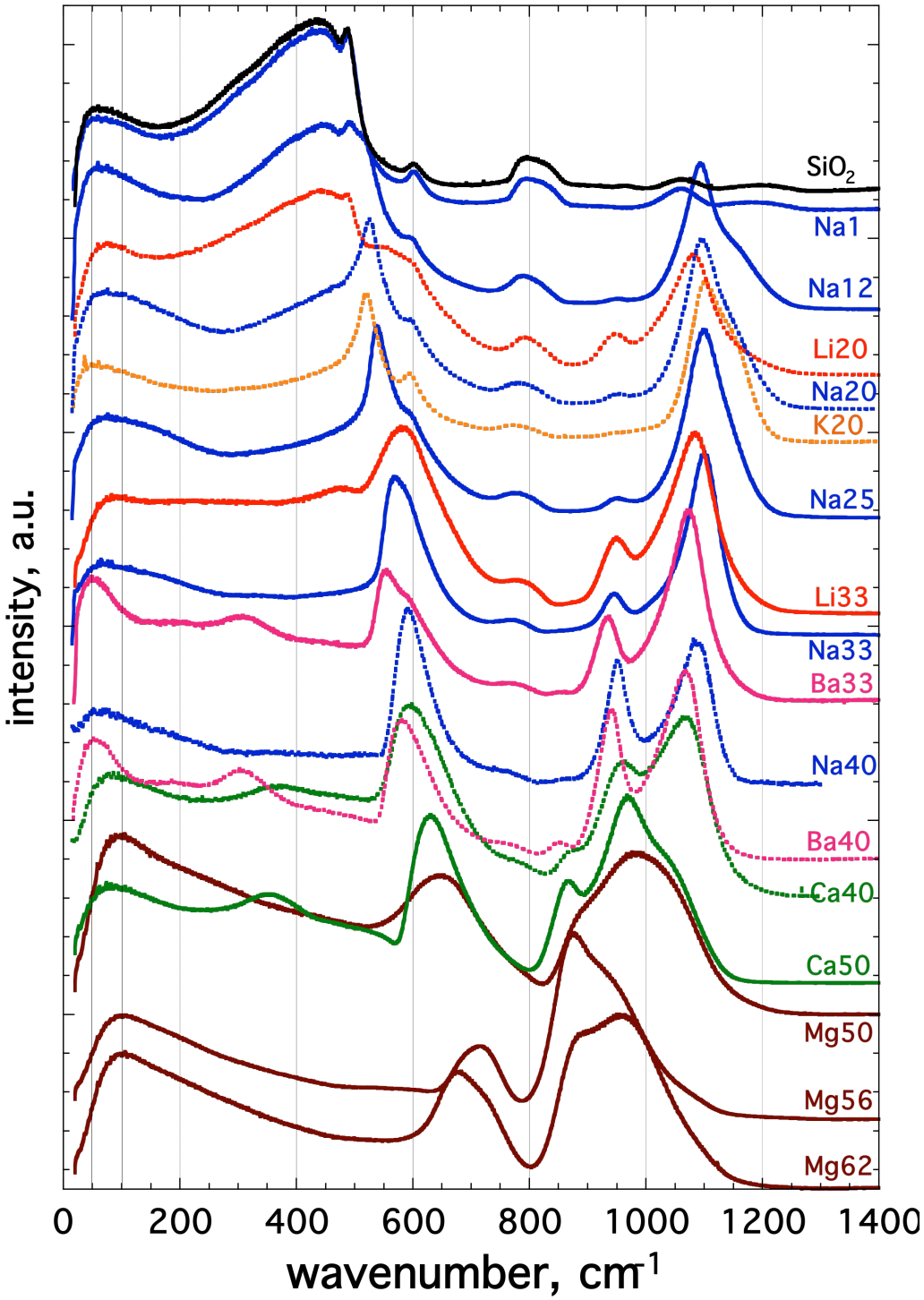

Figure 13: Raman spectra of binary silicate glasses and SiO_2 glass. Raman spectra are labeled as MX, where M=Li, Na, K, Mg, Ca, Ba, and X correspond to the molar fraction of the alkali/alkali earth oxide M. Spectra are normalized to the total area, and vertically shifted.

The effect of alkali or alkaline-earth elements on Raman spectra can be found in more detailed in Neuville et al., (2014). Also, in this chapter, the role of Al, B, iron and volatile elements like H_2O, OH, and CO_2 are described in detailed.

6. Raman spectroscopy for various glass fiber applications

Silica-based glasses provide the backbone of many of today's rapidly expanding photonics applications, which disserve diverse fields such as optical communications, mechanics, electronics, sensor technologies, medicine, and materials processing. Photonic components are paving the way to all-optical devices introducing new methods to miniaturize and integrate components into compact functional systems allowing high processing speeds. For many of these applications, silica based optical fibers and/or bulk glasses are the preferred material, providing both excellent physical and chemical properties such as optical transparency over a wide range of wavelengths, a low thermal expansion coefficient, high mechanical resistance and stable properties over time and temperature.

6.1 Non-Newtonian effect observed by Raman spectroscopy

Silica glass structure is described as a network of interconnected and randomly distributed SiO_4 tetrahedra forming an isotropic material. However, Brückner (1987) has demonstrated that anisotropies and orientations could be introduced into isotropic glass melts through non-Newtonian viscous deformations (Brücker, 1987; Dingwell and Webb, 1990; Simmons et al., 1982, Li and Uhlmann, 1970; Webb and Dingwell, 1990a,b). A non-Newtonian behaviour is described by strain-rate dependant properties, and it could be associated to structural rearrangements occurring in the material (Simmons et al., 1987). Hence, a structural origin of these anisotropies could explain changes in macroscopic property, such as the birefringence of E-glass (silica-based) fiber (Stockhorst and Brückner, 1982) or the different axial and radial elastic responses to an elastic mechanical stress in silica fiber (Champagnon et al., 2014).

The effects of various experimental conditions (drawing speed, tension, temperature, cooling profile) in fiber production have been reported by Lancry et al. (2012), which demonstrated that the resulting fibers have various profiles of fictive temperature, which is known to describe the glass nanoscale structure. The experimentally observed structural modifications, have been also investigated by means of Molecular Dynamics (MD) simulations. Indeed, to study the topological nature of the involved structural rearrangement, Bidault et al. (2015) have developed numerical simulations to study silica glass deformation. The authors focused their attention on the drawing of a silica fiber at high temperature, typically between 2200 K and 2600 K, which is the common stage for most of the manufacturing processes to obtain optical fibers. The use of such a high temperature is crucial, since it has a strong impact on fiber final properties, such as refractive index profile or residual stress. MD simulations have shown that, during the deformation stage, the small silica rings preferentially align, causing a structural anisotropy, referred as "transverse isotropy" by the authors (Bidault et al. 2015) because of different longitudinal and transversal physical properties. The numerical simulation of fiber drawing at 2700 K shown that 3MR (3-Membered Rings of SiO_4 tetrahedra) behave as the most reactive to the traction, with the mean surface that tend to orient perpendicular to the stress axis. This orientation is also preserved in the fiber at ambient temperature. Indeed, during the relaxation, the induced orientation becomes less pronounced because of the decrease of stress and temperature, but still it remains persistent in the fiber at 300 K. On the contrary, high-membered rings (4MR and 5MR respectively, 4- and 5-membered rings) were not greatly affected during the high-temperature stage. However, preferential orientation with a perpendicular-to-stress-axis trend were observed during the relaxation step, which also persists in the fiber at room temperature. 6MR (6-membered rings) orientations, parallel to stress axis, were observed only at high temperatures, since the relaxation stage induced a quasi-uniform orientation distribution. As a result, the numerical simulations show that structural anisotropy in the modeled fiber occurs as result of the persistent orientation of small rings: 3MR, 4MR and 5MR. This structural anisotropy induces a strain-rate dependent properties, and consequently, a non-Newtonian behavior of the glass melt.

This section is focused on the attempt of experimentally reproduce, by Raman spectroscopy, the MD simulations done by Bidault et al. (2015). The same type of anisotropy is evidenced by polarized Raman spectroscopy. For these measurements, first, a 10-mm-diameter silica preform from a Suprasil F300 tube, closed on a MCVD (Modified Chemical Vapor Deposition) lathe, has been drawn in a draw tower at constant temperature (furnace at 2200 K) to form a 1-mm-diameter fiber. To understand this non-Newtonian behavior Raman spectra were recorded using a T64000 Jobin-Yvon® triple Raman spectrometer, in a back-scattering configuration at room temperature. The same small zone located at the edge of a silica glass fiber is probed in both transversal and longitudinal directions, as schematized in Figure 14a. Polarized VV and VH Raman spectroscopy is expected to show differences with probing direction, especially around the R band (440 cm^{-1}) associated to the symmetric stretching of bridging Oxygen, and the D1 (490 cm^{-1}) and D2 (605 cm^{-1}) bands associated to the four- (4MR) and three-membered (3MR) silica rings, respectively (Sharma et al., 1981; Galeener, 1982a,b; Sharma et al. 1985; Pascarello and Car, 1998; Umari and Pasquarello, 2002; Rahmani et al., 2003). The VH settings of the spectrometer are so that neither D1 nor D2 bands are observed in VH spectra (Galeener, 1982b) with fiber in transversal configuration. VV Raman spectra are deconvoluted using a Levenberg-Marquardt algorithm. After a Long correction (Long 1977; Neuville and Mysen, 1996), six bands between 200 and 670 cm^{-1} are progressively adjusted: four bands with a Gaussian, and D1 and D2 bands with a linear combination of a Gaussian and a Lorentzian (to approximate a Voigt function). In fact, the fit converges toward the only need of a Gaussian for D1 and a Lorentzian for D2. These bands are then fixed to fit a seventh Gaussian, and the Boson peak around 60 cm^{-1} with a log-normal function (Malinovski and Sokolov, 1986; Dianoux et al., 1986; Hehlen et al., 2000, 2002).

Longitudinal and transversal VV and VH Raman spectra of the fiber are superimposed in Figure 14a. Classical deconvolutions of Longitudinal and Transversal VV spectra are represented in Figures 14b and 14c, respectively. Both deconvolutions have a correlation coefficient R2 very close to 1. Zoomed views on D1 and D2 bands are represented in Figures 14d and 14e, respectively. Assuming an isotropic glass, an intensity change in Raman spectra is related to a ring population change, as shown by Alessi et al. (2012) between D1 and D2 bands of the preform and the fiber, or by Hehlen (2010) between D1, D2 and R bands upon silica densification. However, the Raman response of a given molecular group is described by its polarizability, which is by nature a tensor. So, depending on the probing direction of the laser, a structural anisotropy commonly leads to an intensity change of some Raman bands, as shown for instance in oriented polymers (Kozanecki et al., 2004). This change is clearly visible in the VH spectra. All settings of the spectrometer being unchanged, whereas there is neither D1 nor D2 peaks in transversal configuration, it is interesting to see the D2 band reappearing in longitudinal one, and the curve shapes differing between 300 and 600 cm^{-1}.

Intensity changes are not so obvious in the VV spectra, but reproducible frequency lowerings are measured in transversal configuration. The mean frequency of the R band, related to 5MR and larger, is lowered by 0.9 cm^{-1}. The D1 peak related to 4MR is lowered by 0.7 cm^{-1}. The D2 peak related to 3MR shows a similar trend with the transversal curve always 0.7 cm^{-1} on the left of the longitudinal one between 580 and 620 cm^{-1}. These three experimental determinations, higher than spectral resolution of the triple Raman spectrometer, are clearly correlated to the anisotropy created by 3MR, 4MR and 5MR at the end of the drawing process simulation.

In the real fiber, the same rings of the same area are seen and probed in two different directions, which are perpendicular to each other. Due to the transverse isotropy, resulting Raman responses differ, but in frequency. As explained by Hehlen (2010), Deschamps et al. (2009) and Champagnon et al. (2008), this frequency variation is linked to the stress undergone by the Si-O-Si bond. Thus, since the elastic constant matrix of the modeled fiber reflects anisotropy, the stresses induced by a

transverse or a longitudinal probing on these Si-O-Si bonds of the same area differ from one another, and this difference manifests itself in the frequency variations observed in the VV Raman spectra. Similar variations of some Raman bands, at 401 cm^{-1} and 807 cm^{-1}, lowered by 1.4 cm^{-1} and 3.0 cm^{-1} with probing direction, respectively, have been reported by Masso et al. (1970) in α-quartz, a silica crystal structured by only 6MR. The fact that bands are below 1000 cm^{-1} seems to corroborate that the anisotropy is only induced by the rings.

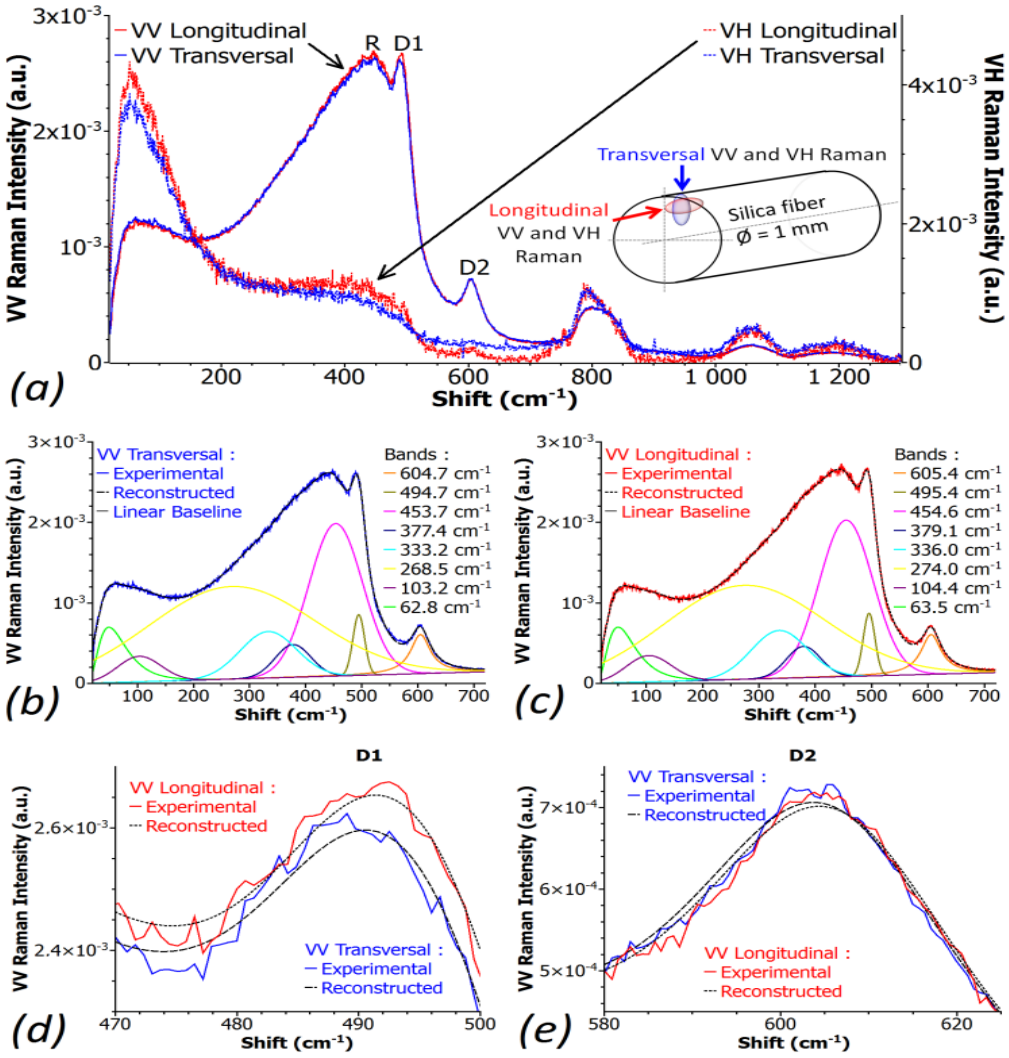

Figure 14. Polarized Raman configurations and spectra. (a) A small zone located at the edge of the fiber is probed in two different directions. Raman ellipsoids are oversized for clarity. VV (solid lines) and VH (dotted lines) Raman spectra of the fiber explored in longitudinal (red) and transversal (blue) directions; (b) VV Longitudinal deconvolution (R^2 = 0.99941); (c) VV Transversal deconvolution (R^2 =0.99936); (d) zoom on D_1 band; (e) zoom on D_2 band. Raman spectra were recorded one after the other in the same conditions.

Such a study is only possible because the T64000 spectrometer is a particularly accurate triple spectrometer, with a resolution greater than 0.5cm^{-1}. It is obvious that with a simple Raman spectrometer, it is not possible to carry out such a study. In the same way, the Raman spectra acquired in VH condition are ten times less intense than the spectra acquired in VV. Hence, this type of study is very rare in the literature, because difficult to achieve, but it allows to bring important elements on the deformation of the rings subjected to uniaxial deformations that can

perfectly well correlate with non-Newtonian behavior already observed on some glass fiber (Dingwell and Webb, 1990).

6.2 Loss reduction in telecommunication optical fibers

One of the most common applications of Raman spectroscopy in optical fibers is related to the reduction of their optical attenuation. Indeed minimizing the optical losses in optical fibers is a recurrent target for fiber manufacturers. It is well known that the fictive temperature T_f characterizes the glass structural disorder (Tool, 1946) and is linked to glass properties (Lancry et al., 2012) such as density, mechanical fatigue resistance or Rayleigh scattering loss. From optical fiber manufacturing point of view, monitoring the fictive temperature (mostly through glass vibrational signature) is thus a quick and reliable way to optimize the manufacturing process (Kim et al., 2001; Helander et al.; 2004) in order to reduce the Rayleigh scattering loss, which is the major source of loss in telecommunication optical fibers. For a single mode telecommunication fiber, this corresponds to 90% loss at 1310 nm and 80% at 1550 nm (e.g. 0.16 dB/km for a total of 0.19 dB/km).

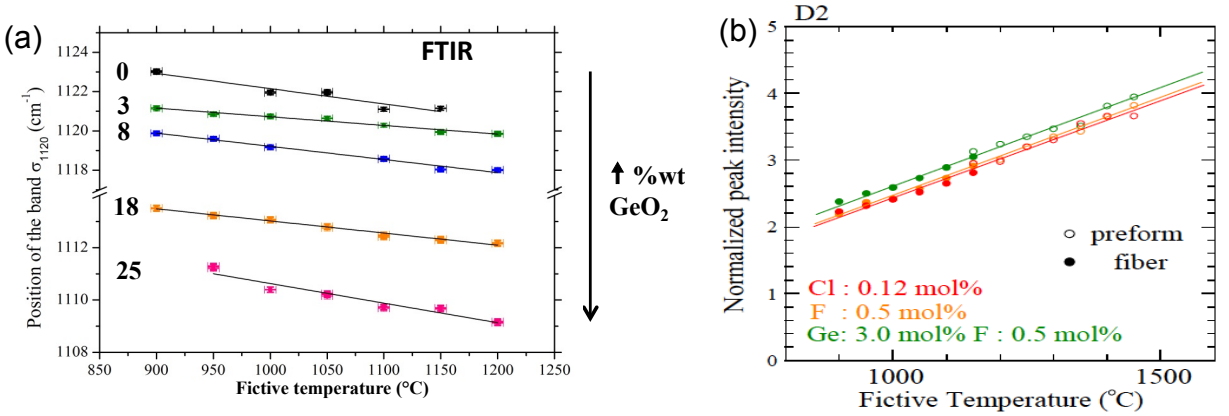

Figure 15. (a) Asymmetric stretching band wavenumber of various germanosilicate fibers as a function of fictive temperature T_f, (b) D_2 band normalized intensity of various preforms (empty dots) and fibers (full dots) as a function of T_f for typical fiber materials: Cl-doped SiO_2, F-doped SiO_2 and Ge-F codoped SiO_2.

As review recently the fictive temperature T_f of silica based glasses can be determined easily and in a reliable manner by Fourier Transform Infra-Red spectroscopy or Raman scattering spectroscopy (Agarwal et al., 1995). In these methods, scientists use an empirical relation that exists between the wavenumber, width or intensity of silica structural bands and the fictive temperature. However, one problem is that the features of the silica bands (position, intensity and width) vary not only with T_f but also with the elaboration process and the material composition (Lancry et al., 2012, Lancry et al., 2007). This is an issue as the chemical composition of a fiber is not constant throughout its cross section but varies with the designing of the desired refractive index profile for a targeted application e.g. Single Mode Fiber (SMF), Multi-Mode Fiber (MMF), Pure Silica Core Fiber (PSCF), Dispersion Compensating Fiber (DCF), Dispersion Shifted Fiber (DSF). Thus, calibration curves between T_f and the IR band peak characteristics (position, intensity, width) are needed for each material composition (F, P, Cl, Ge, Boron…). Some typical examples of such calibration curves are reported above in Figure 15.

In the literature, two approaches have been used to reduce Rayleigh scattering loss in silica-based fibers via a reduction of T_f as recently review in (Lancry et al., 2012).; namely optimizing the core/cladding chemical compositions (Saito et al., 2004) and/or optimize the thermal conditions for fiber drawing (Sakaguchi and Todoroki, 1998; Sakaguchi, 2000). Physically, using these methods, the idea is to reduce the structural relaxation time τ. This should result in lower T_f and thus lower Rayleigh scattering coefficient R_ρ due to density fluctuations. The main approach

is to accelerate the structural relaxation of the core for lowering T_f. Indeed, τ_{core} can be shortened by an appropriate doping of the core but also of the fiber cladding. Following this path, T_f reduction in single mode fibers has been extensively studied by Sumitomo and NTT companies by means of Chlorine or Fluorine doping (Kakiuchida et al., 2003a,b).

6.3 High Temperature optical fibers sensing and underlying microscopic mechanisms

Improving fiber Bragg grating (FBG) sensors to operate in harsh and extreme environments is a rapidly growing field of research (Mihailov et al., 2017; Canning et al. 2010). A new generation of devices that operate in these extreme environments (particularly those above 800 °C), including with additional challenges such as radiation and intense optical fields (e.g. high power lasers), must be capable of withstanding gradual annealing and degradation, or aging, over a suitable period of time while preserving their intrinsic advantages (multiplexing capabilities, electromagnetic immunity, low intrusiveness, mechanical reliability) over other, conventional technologies such as thermocouples. Much of the answer to improving these technologies lies with optimizing inherent glass structure and properties, particularly viscous flow, chemical and structural migration and stress relaxation and fundamentally recognizing the opportunities multi-materiel systems provide. Overall, FBG regeneration (Canning et al., 2008) s one of the two main current approaches (the other being femtosecond laser writing, Mihailov et al., 2017) that can enable photonic technologies to operate in such harsh environments at elevated temperatures. In its simplest recognizable expression, regeneration involves the annealing and resurrection of a structure patterned into a glass through optical or thermal treatment. This pattern, or seed structure, has changed the thermal or optical history of the glass so that whilst the annealing is identical in all areas, the local response is different, equivalent to a local variation in quenching. FBG regeneration has been interpreted (often without recognizing relaxation and the multi-material system being used) in different ways (Canning et al., 2010) including dopant chemical migration (fluorine evolved into oxygen in order to explain performances above 900°C for example), crystallization and glass structural changes. One local approach to study structural relaxation is to spectroscopically follow structural changes that are associated with a density change. Here we will provide a recent example where Raman micro-spectroscopy was used to investigate the mechanisms of FBG thermal regeneration in B-codoped germanosilicate GF1 optical fibres (Lancry et al., 2018).

As Figure 16(a) shows minor changes for D_2 peak at $\nu \sim 605$ cm^{-1} were observed in the core when comparing the pristine fiber and the thermally treated one. Examining the D_1/D_2 amplitude ratio shown in Fig. 16(b), we can see a spectacular increase everywhere of the ratio revealing a structural relaxation characterized by a decrease in glass density (expansion has occurred). Note there is also a significant decrease of D_2 within the inner cladding after thermal treatment that is consistent with compressive stress relaxation. However, whereas the relaxation of the initial tensile stress in the core should leads to a decrease of D_1/D_2 ratio, we instead observe the signature of glass expansion.

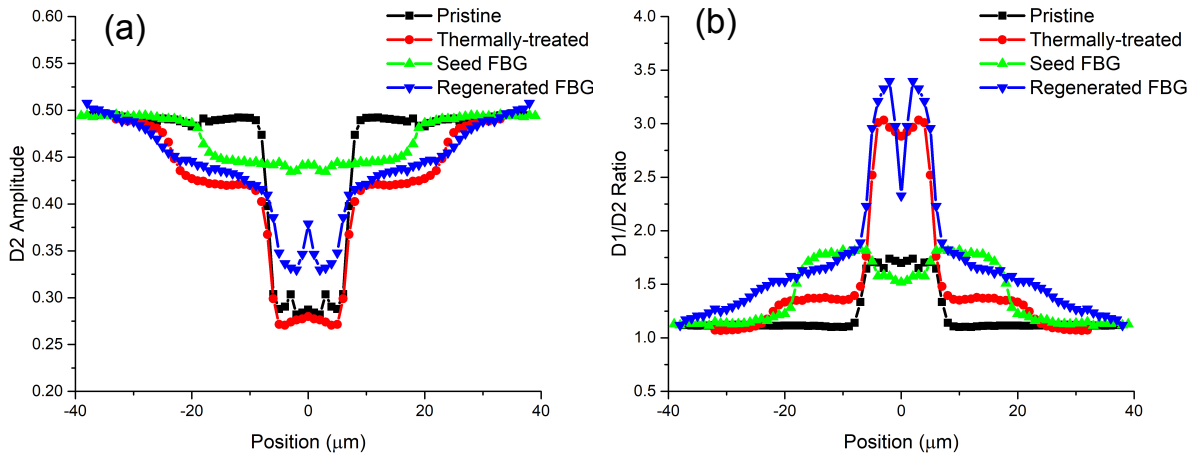

Figure 16. Raman spectra of the B-codoped germanosilicate GF1 fibre core: pristine, seed Fiber Bragg Grating and regenerated FBG. Thermally-treated GF1 fibre without any irradiation is also shown for sake of comparison. (a) D_2 amplitude and (b) D_1/D_2 ratio along fiber cross-section. (Lancry et al., 2018)

Now comparing the seed UV FBG and the pristine fiber, we can see an increase for both D peaks; i.e. D_2 at $\nu \sim 605$ cm^{-1} in Fig. 16(a) and D_1 (not shown here) in the fiber core and a slight decrease of the D_1/D_2 ratio, which reflects the expected UV-induced densification. In contrast, we observe the signature of glass expansion within the inner cladding of the seed UV FBG. After regeneration both D peaks are observed to strongly decrease in height (and in area as well) when compared to the seed UV FBG. Gaussian decomposition, however, reveals an increase of the D_1/D_2 ratio in the fiber centre after regeneration – likely revealing an expansion. In addition there is a slight change of the shape of the main band around 390 cm^{-1} (not shown here) that indicates an increase of the 6-membered rings. Significantly, high changes are also observed within inner cladding even compared to the thermally treated fiber. In addition, Ramen profiles indicate substantive increase of the inner-cladding dimensions.

6.3 Irradiations effects investigated by Raman spectroscopy

Over the last two decades laser-induced Δn profiling in SiO_2 glasses was widely used for production of in-fibre/waveguide Bragg grating-based (BG) optical devices for photonics industry (Lancry et al., 2013). Irrespective of the type of irradiation, these changes are based on point defects and structural changes (observed in vibrational spectroscopy and in particular Raman spectroscopy) induced by irradiation. In particular, a phenomenon observed from the first studies received a lot of attention because of its quasi-universal nature (under laser irradiation or radiative environment, under hydrostatic loading, under shock, etc ...) but also its potential in the field of optics for light guidance or the manufacture of integrated optical functions. This is a phenomenon of permanent densification of silica. Indeed silica glasses densification is commonly observed under various kinds of irradiations employing neutrons, ions, electrons, X rays, γ rays, UV laser light and IR femtosecond laser irradiations, with energies ranging from keV to MeV (Primak, 1958; Vanelstraete and Laermans, 1988; Seward et al, 1997; Primak and Kampwirth, 1968; Devine, 1994; Spaargaren et al., 2000; Barbier et al., 1991;). Such kind of modification occurs also after sub-bandgap irradiations with UV or Vis-IR femtosecond lasers. The experimental fact that fused silica undergoes densification upon prolonged exposure to high-energy radiation is well documented in the literature. About 50 years ago, Primak (1958) reported permanent densification in SiO_2 under irradiation with neutron, electron, and γ-ray exposures. Therefore, there have been a number of experimental studies describing the permanent densification of silica or silica-based

glasses under various kinds of thermo-mechanical solicitations including irradiations and especially in glass fiber materials.

6.3.1 Glasses in nuclear environments

The knowledge of the glass structure in some simple systems before and after irradiation is a prerequisite for understanding the structural evolution of nuclear glasses under irradiation during long term storage but also to understand the behavior of glass fiber in some condition. Studies on irradiated glasses have been previously published on simple system like SiO_2 (Devine, 1994; Ollier et al., 2017; Ollier et al., 2019), or on multicomponent glasses like borosilicate glasses (Boisot et al., 1999) and on some aluminosilicate (Neuville et al., 2003).

In all sort of glasses, β-irradiation produces: -i) an increase of the network polymerization relative to the non-irradiated samples, -ii) an increase in concentration of molecular O_2, clearly visible at 1550 cm^{-1} and -iii) a decrease of the average Si-O-Si bond angle (Boizot et al., 1999, Balan et al., 2001, Neuville et al., 2003). For example, the Figure 17 shows calcium aluminosilicate glasses before and after β-irradiation.

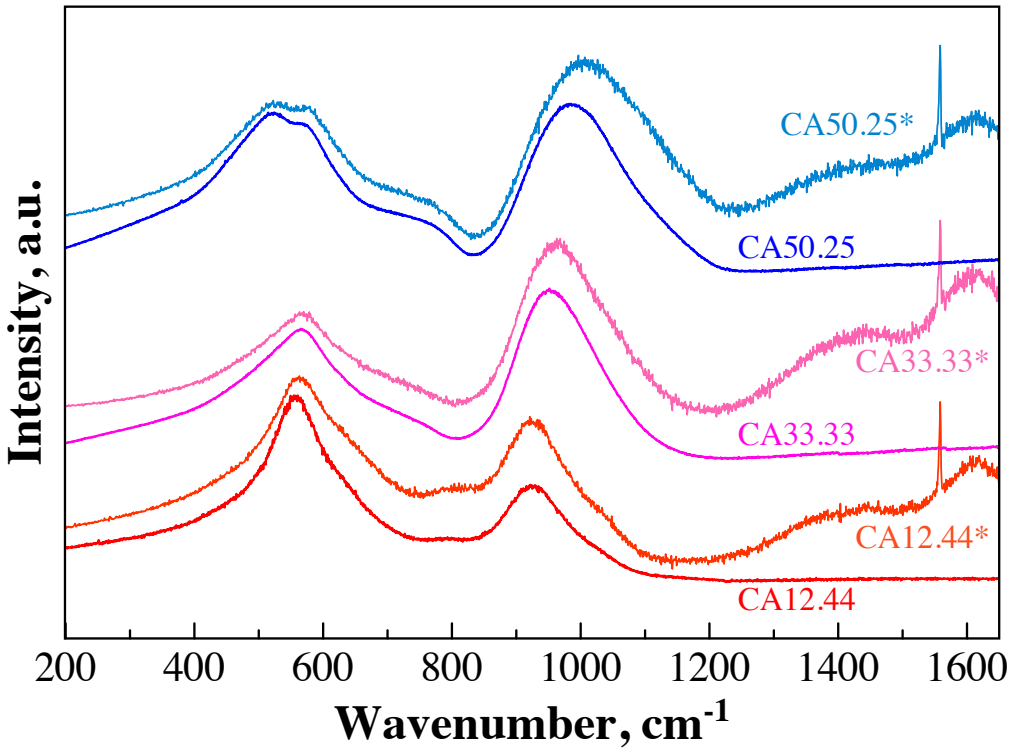

Figure 17. Raman spectra of calcium aluminosilicate glasses before and after(*) irradiation. Samples of 0.5 mm thick were β-irradiated using 2.5 MeV electrons generated by a Van De Graaff accelerator at 20 µA. The temperature of irradiation was maintained around 50 °C. The dose integrated in the CAx.y glasses is $3.8x10^9$ Gy where X is the content of SiO_2, Y the content of Al_2O_3 in mole % (CaO= 100-(X+Y)). The Raman measurements were carried out on a T64000 Jobin-Yvon confocal microRaman spectrometer, see Neuville et al. (2003) for more detail.

All irradiated spectra, marqued with *, show a shift in frequency for the prominent peak from 900 to 1050 cm^{-1}, as the silica content increases, which can be attributed to an increase of the network polymerization. The glass network becomes more connected as Al is substituted by Si since the proportion of Q^3 and Q^4 species increases (Neuville and Mysen, 1996, Neuville et al., 2004, 2006). In the irradiated glasses, the shift of the Raman band at 520 cm^{-1} has been interpreted as a decrease of the average T-O-T bond angle (Boizot et al., 1999).

This observation is similar to the effects induced by a glass densification and suggests a decrease of the average size of the TO_4 membered rings. Furthermore, the small shift of the large

band around 900-1050 cm^{-1} indicates that the glass network becomes more polymerized after irradiation. This is confirmed by an increase of the Q^3/Q^2 ratio after irradiation, as determined by the deconvolution of the Raman spectra. We also observed than the proportion of the Q^4 species increases. The migration of the calcium can be responsible for this structural change (Boizot et al., 1999; Neuville et al., 2003).

The presence of the intense peak at 1550 cm^{-1} in the Raman spectra of irradiated glasses is characteristic of molecular O_2 and was also observed in irradiated borosilicate glasses (Boizot et al., 1999). The production of molecular O_2 is a consequence of the polymerization increase under irradiation because this process forms excess oxygen atoms within the glass structure. The proportion of O_2 does not seem to be dependent on the silica content.

Raman spectrometry studies on the structure of irradiated or non-irradiated glasses are very important because they can be performed in situ and / or ex situ. This type of study can make it possible to understand the aging of an optical fiber that could be embedded on a satellite object, for example a satellite, a space shuttle. This could bring important elements to understand the aging and therefore the obsolescence of a fiber. However, some studies are currently available and they are mainly focused on nuclear waste storage glasses, but few studies are available on optical fibers. It would be interesting, for example, to study by Raman spectrometry the effect of β and neutron irradiations on $Ge_{100}Si_{(100-X)}O_2$ glass optical fibers.

6.3.2 Reduction of optical fibers radiation resistance for harsh environment applications

The use of silica glass optical fibers in radiative environments is of major interest to the civil, military or space fields, due to the numerous advantages of the fibers and in particular their electromagnetic immunity, wide bandwidth, light weight and low volume. These optical fibers can be used as tools for transmitting information, as sensors or as diagnostic elements. However, radiation of sufficiently high-energy incident on a waveguide or an optical fiber will break or ionize bonds in the glass structure and produce defects centers. These defects can absorb light propagating in the optical waveguide, resulting in an increase of the linear attenuation or so-called Radiation-Induced Attenuation (RIA). Many studies have been performed on various types of passive optical fibers in order to understand the RIA effects, to determine the origin of these phenomena and to find treatments for improving the resistance of optical fibers to ionizing radiations (Girard et al., 2013; Berghmans et al., 2008). Further, it is believed that an optical fiber, which has point defects and defect precursors in its bond structure is more sensitive to ionizing radiation and is more likely to retain structural damage caused by radiation. Hence, efforts to produce radiation resistant optical fibers have focused on: i) Producing a fiber from materials which form "strong" bonds by F-doping (Hayami, 1991; Ishiguro et al. 1992), usually attributed to Si-F bond formation and the reduction of 3 and 4-membered rings, which are detected using Raman spectroscopy (Henschel et al., 2011; Morana et al., 2015); ii) Producing a fiber which is low in pre-existing defect concentration. According to Hayami (1991) the reduction of chlorine impurities and OH groups leads to a reduced RIA in the visible domain when the fiber is exposed to a γ-ray source for a total dose of 3.1 kGy. iii) Other methods include pre-irradiation, hydrogen passivation treatments and a combination of H_2 and pre-irradiation. Another possible approach is to adjust the thermal processing of the glass during or after the fabrication process to tailor the glass fictive temperature. Galeener et al. (1993) has reported a reduction of both pre-existing defects including 3 and 4-membered rings and the E' defect generation rate when T_f is lowered. Yamaguchi et al. (2003) showed that the number of self-trapped hole centers (STHs) created at 77K by identical ArF laser irradiations became greater when silica or F-doped samples (Wang et al., 2005) were forced to have higher fictive temperatures. In all of these methods Raman spectroscopy is a key tool to follow defects, OH groups or structural changes.

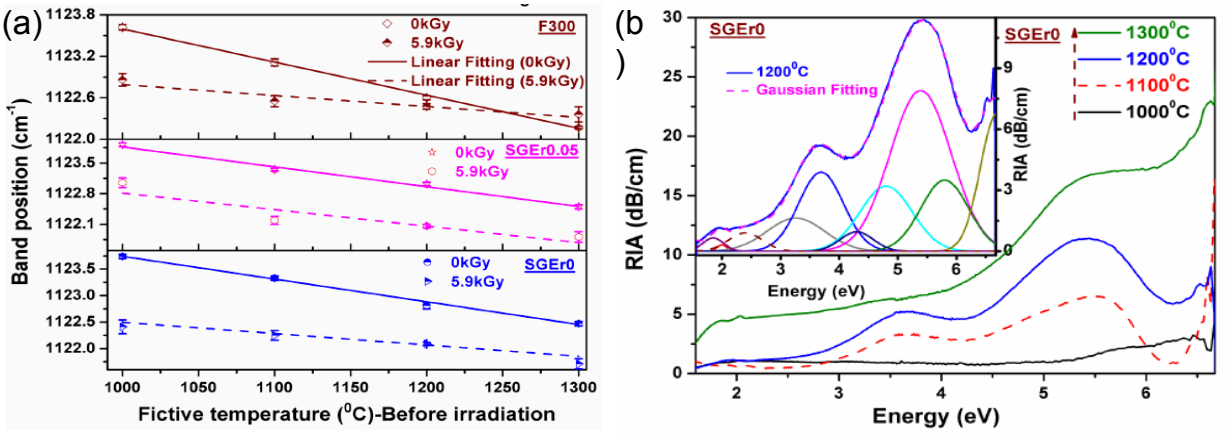

Figure 18. (a) Asymmetric stretching band wavenumber $\sigma_{\text{Asym Si-O-Si}}$ of SGEr0 (solgel silica), SGEr0.05 (Er doped solgel) and F300 silica lasses as a function of fictive temperature T_f, before and after γ-irradiation. (b) RIA spectra of solgel silica glass for different fictive temperatures. Inset shows the typical deconvolution spectrum for T_f=1200°C. (Hari Babu et al., 2016)

A recent example of such approach is shown below in solgel silica optical fibers preforms (Hari Babu et al., 2016). Before γ-irradiation, $\sigma_{\text{Asym Si-O-Si}}$ is plotted against T_f as shown in Fig. 18(a). In the investigated T_f range and for all silica samples namely (F300 silica rod, solgel silica and erbium doped solgel silica fiber preforms), when increasing the fictive temperature, asymmetric stretching band is shifting towards lower wavenumber. After 5.9kGy γ-irradiation, a lower frequency of Si-O-Si asymmetric stretching band in all studied silica glasses can be found whatever the T_f may be. This indicates that a slight reduction of Si-O-Si bond angle variations takes place as a result of γ-irradiation. The most plausible explanation of the band frequency decrease, as compared to before γ-irradiation, could be an increase of the fictive temperature (and likely of the glass density) under γ-irradiation. The radiation induced attenuation (RIA) spectra of solgel silica glass are reported in Fig. 18(b) according to the fictive temperature (1000-1300°C). EPR analysis in combination with other spectroscopic techniques (Raman, UV-Visible absorption and photoluminescence) show clearly that a lowering of the fictive temperature results in a lowering of defect concentration (SiE'_γ and peroxy radicals) before and after irradiation and so to a smaller RIA. Based on these results, it is clear that a better control of fictive temperature should reduce the generation rate of most point defects in high purity silica glasses and especially in optical fibers including F-doped or Cerium-doped radiation resistant fibers. A combination of these two approaches (e.g. specific doping and T_f reduction) is promising in terms of achieving further radiation resistance for silica-based optical fibers. Another important point is that optical fiber core doping needs to be associated with optimized drawing conditions and careful fiber design in order to favor the structural relaxation of the fiber core, with the main objective to reduce its fictive temperature.

6.3.3 Femtosecond laser processing of glasses for photonics applications

Ultrashort laser pulses are known as intriguing tool for materials processing with outstanding precision as required in a growing number of technological fields. In particular for glasses such as fused silica, the nonlinear absorption mechanism allows to transfer the pulse energy to a confined volume within the focal region (Poumellec et al., 2011). The resulting modifications range from

isotropic refractive index changes, birefringence due to self-organized oxide composition (Lancry et al., 2013]) to microscopic voids with densified shell. Moreover, when using high repetition rates the laser pulses act as a local heat source leading to temperatures well above the melting temperature of the glass (Eaton et al., 2005). After rapid cooling (typ. >10^6 K/s) the molten glass resolidifies allowing for the local bonding of glass interfaces but is also possible to crystallize glasses or to imprint permanent densification through local fictive temperature changes (Zimmermann et al., 2017), which can be further exploited for optical applications including fiber optics components and sensors.

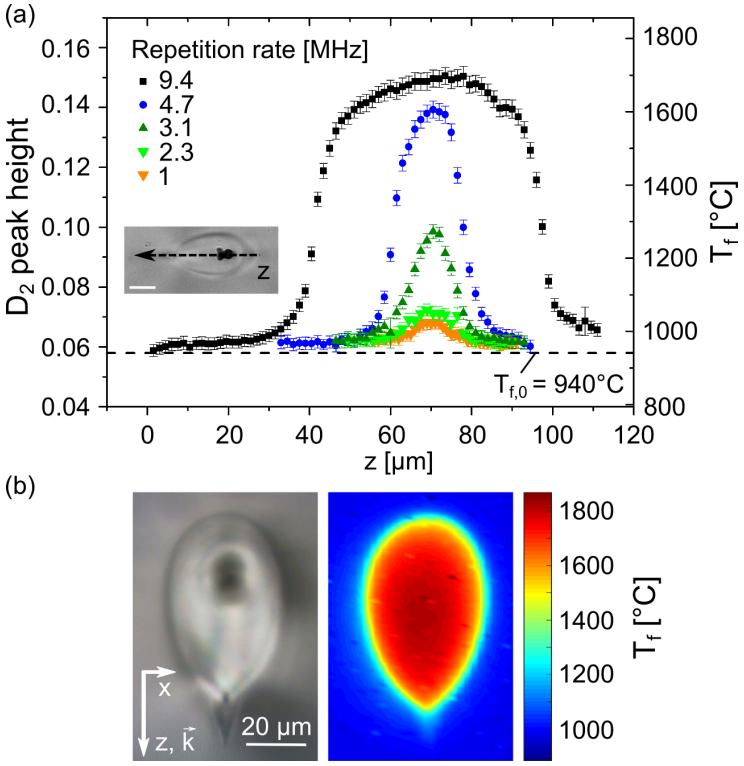

Figure 19. Results of the Raman measurements. (a) D_2 peak height (left axis) and corresponding fictive temperature (right axis) as function of the longitudinal cross section (inset shows an optical micrograph with indication of the measurement trace). (b) Microscopic optical image and corresponding map of the fictive temperature for a laser-induced modification inscribed with 9.4 MHz, 150 nJ and 1000 pulses per laser spot. The arrow indicates the propagation direction of the laser. (Zimmermann et al., 2017)

As an example IR femtosecond laser-induced modifications in silica inscribed with different repetition rates were analyzed by Raman spectroscopy to evaluate the consequences of increasing heat accumulation on the resulting fictive temperature. Figure 19 shows the measured D_2 peak height and corresponding T_f of the longitudinal cross section deduced from calibration curves made on thermal-treated samples (Lancry et al, 2011). For all heat affected zones (HAZ) there is a significant increase of fictive temperature compared to pristine glass. Interestingly, T_f scales with the laser repetition rate and reaches values up to 1700°C at 9.4 MHz. The longitudinal profile illustrates that the highest fictive temperatures can be obtained in the central region and radially decreases from the center to the rim of the HAZ. Based on the increase in fictive temperature it is also possible to evaluate the change in volume of the material within the focal volume. The relative free of stress volume change (opposite to material density - ρ) due to fictive temperature change

is $-\frac{1}{\rho}\frac{\Delta\rho}{\Delta T_F} = -5.7 \cdot 10^{-6}$ and is negative in case of silica (R le Parc et al., 2006). For example, we obtain an increase ΔT_f of about 750 K for a repetition rate of 9.4 MHz within the heat-affected zone (HAZ) resulting in a free of stress densification of 5.10^{-3}.

6.4 Permanent densification of glasses investigated by Raman spectroscopy

One common way is to follow the structural changes that indicate a density change using Raman spectroscopy and particularly the so-called 'defect' bands. Historically, the D_1 and D_2 bands, located at 490 and 605 cm^{-1} respectively, have been first interpreted by Sharma et al., 1981 and Galeener, 1982a,b as being 'breathing' vibration modes of four and three-membered rings respectively in the material as discussed in details in section 6.1. As a first approximation, and for a given composition, a change in the intensity or the area of these bands indicates a modification in the rings statistics. As a result, many authors consider that the Raman D_1 and D_2 bands record matter densification in glass.

In pure silica glasses a permanent increase of density (densification) occurs after compression, with the density of a SiO_2 glass approaching the one of the SiO_2 crystal, by increasing up to ~20-21% (Bridgman and Simon 1953, Susman et al. 1990; Cohen and Roy 1965). It has been experimentally verified that below 28GPa, the densification is due to structural changes (intertetrahedral angles distribution and the ring statistic) without variations in Si-O coordinations (Meade et al., 1992; Sugiura et al. 1997, Deschamp et al. 2013). Furthermore, molecular dynamics calculations also support these considerations ascribing the densification to modification of T-O-T angles and ring populations, rather than to an increase in coordination (Jin et al., 1993).

Raman spectroscopy is very sensitive to structural variations, thus, it is an optimal tool to follow the structural evolution of glasses upon compression, and to determine structural modifications both in the short- and medium-range order. For example, Deschamp et al. (2013) studied SiO_2 glasses densified under hydrostatic pressures from 9.8 up to 26 GPa. The authors provided a Raman-density calibration curve, and also identified the elastic yield under hydrostatic pressure, at room temperature, to be around 9 GPa for a pure SiO_2 glass (Deschamp et al., 2013).

Raman spectroscopy has been also used to identify the residual densification, after indentation tests, and to characterize the plastic behaviour of amorphous silica (Perriot et al. 2006). The induced densification on a silica plate by a 2kg Vickers diamond indenter was studied by Raman spectroscopy, both on the imprinted surface and on the cross-sections of the indents. By correlating the defect lines D_2 to the densification ratio (following the work of Sugiura et al. 1997) the authors estimated the residual densification and by using the variations of the defect lines, they redraw a 3D map of the indentation-induced densification (Perriot et al. 2006).

However any amorphous network has a range of densities for the same number of rings structures (and bond angles) so in of itself such a statement is not necessarily correct. The D bands measure local structures and therefore whilst they can correlate with local densities that do not mean they have to correlate with bulk densities and here are three practical examples in fiber materials of breaking equivalence between these indicators and macroscopic glass density.

Thermal relaxation of densified silica: A first example can be revealed from mechanically densified SiO_2 glasses, obtained from different pressure and temperature routes which have been annealed over a wide range of temperatures far below the glass transition temperature (500°C-900°C) by Dominique De Ligny coworkers. In situ micro-Raman spectroscopy was used to follow the structural evolution during the thermal relaxation. Cornet et al. (2017) experiments have also shown that the concentration of 3 membered rings (D_2 band) is not directly related to the densification rate. They show a non-monotonous evolution of the area under the band D_2 (normalized with respect to the total surface of the spectrum between 200 cm^{-1} and 900 cm^{-1}) as a function of the degree of transformation during the relaxation several densified samples. The area under the band D_2 undergoes an increase before decreasing, while the rate of densification decreases monotonously. Thus the densification rate would be essentially driven by other factors, such as the opening of Si-O-Si angles and the overall rings statistics and not on these local indicators.

Fictive temperature in GeO_2-SiO_2 optical fiber preform: Another example from the fiber community is related to a comparison between silica and germanosilicate glasses (from 5 up to 25w% in GeO_2). As shown in Fig. 20(b), these glasses present opposite behaviors with regard to the variations of their density with fictive temperature T_f (higher T_f higher density for SiO_2). For these two glasses, the Raman D_1 and D_2 band intensities increase with increasing fictive temperature, indicating an increase of the proportion of 3 and 4-membered rings (see Fig. 20). This leads to the following result: the higher the density is, the higher the Raman defect bands intensities are for the pure silica glass, but the opposite behavior is observed in $25GeO_2$-$75SiO_2$ glass (Heili et al, 2016). As a consequence, if D_2 band intensity may be used in pure silica as an indicator of density, as it is commonly done in the literature, this cannot be extended to any binary glasses and/or any conditions. The D bands measure local structures and therefore whilst they can correlate with local densities that does not mean they have to correlate with bulk densities.

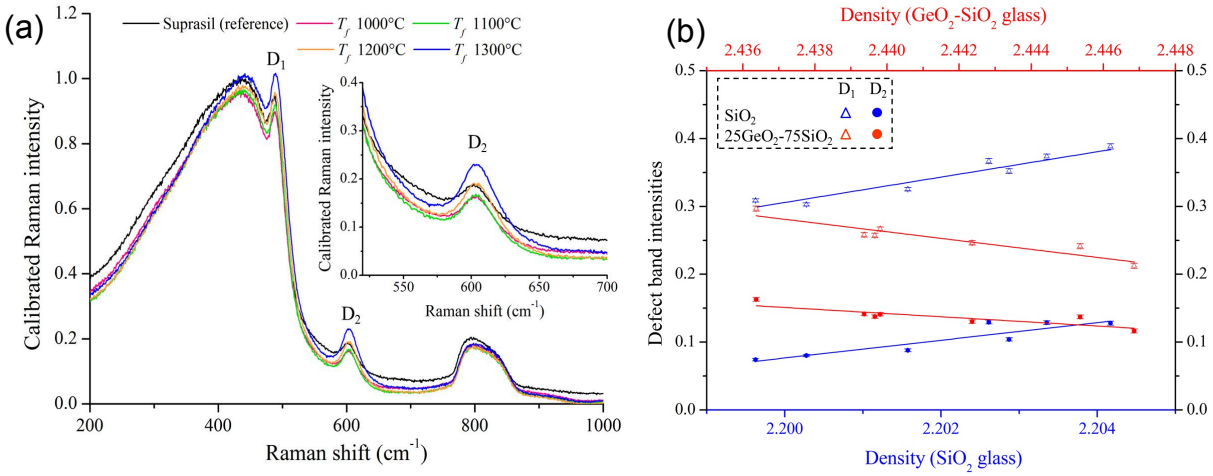

Figure 20. (a) Raman spectra performed at room temperature of PCVD $25GeO_2$-$75SiO_2$ glass samples with fictive temperatures of 1300, 1200, 1100 and 950°C. (b) Calibrated intensities of D_1 and D_2 bands as function of PCVD glass densities: pure silica SiO_2 (blue) and $25GeO_2$-$75SiO_2$ (red). (Heili et al, 2016).

Irradiation of densified silica: In a recent publication, the authors examined the "relaxation properties" of pre-densified synthetic fused silica glass under 2.5 MeV electron irradiation with high-integrated dose (Ollier et al., 2017; Ollier et al., 2019). The densification of the glass was obtained by hot compression (5GPa-350°C and 5GPa-1000°C). After irradiation of hot compressed silica, the Raman spectra display a significant increment of 4 and almost 3-membered rings whereas they exhibit a glass density reduction. In contrast, the wavenumber and the FWHM

of the R band peaking at 440 cm^{-1} appears to remain correlated to the silica glass density for all investigated samples. In this work that the correlation between density and D_2 intensity remains valid until silica density remains lower than 2.26. This is consistent with many publications, which reports an increase of the D_2 band area with the dose (Gavenda et al., 2015) (for compaction rate < 3%, 5 keV electrons irradiation). Most of laser (IR-fs un type I regime or UV ns) related silica studies also (where density variation is less than 1 %) mention a D_2 band increase that is assigned to a glass densification.

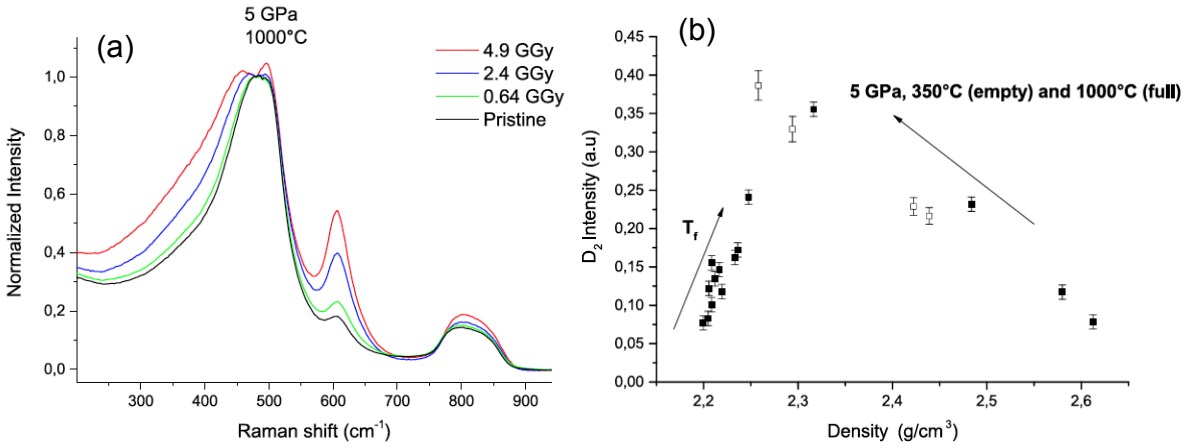

Figure 21. (a) Raman spectra evolution with the integrated dose of (5GPa, 1000°C) samples. (b) Raman D2 band intensity as a function of density for HP-HT and T_f samples.

These measurements confirm that D_2 increase cannot be considered as an absolute marker of glass densification. It remains only true in SiO_2 when the density is below its equilibrium value around 2.26. Up to date, the wavenumber and FWHM of the R-band however seem to be a more relevant densification marker in amore general approach. The spatial resolution and the high frequency resolutions achievable by Raman spectroscopy make it a very powerful and versatile tool to correlate macroscopic properties (density, mechanical behaviour) to variations at the sub-nanoscale.

7. Volatiles, crystallisation, nucleation

7.1 Volatiles in glasses

Gas, volatile elements and water have a strong Raman signature and are generally easy to investigate. However, it is more complicated to study dissolved gases and volatiles in glasses. CO_2, H_2O, N_2, SO_4 dissolved in glass have been studied by several authors (Verweij et al. 1977; Mysen and Virgo 1980, Thomas 2000, Behrens et al. 2006, Roskosz et al. 2006, Le Losq et al, 2012, 2013, Thomas et al. 2008; Tsujimura et al., 2004; Lenoir et al. 2009, 2010, Amalberti et al., 2011a,b). Recently, Le Losq et al. (2012) have proposed a new baseline correction to quantified the water concentration and speciation in silicate glasses and melts.

To determine the water concentration, Le Losq et al. (2012) used a robust reproducible method to smooth and interpolate a baseline below the regions of interest, particularly in the silicate part of the Raman spectrum. They used *general cross validated splines* which perform an optimized smoothing and interpolation of a smooth function with known random noise (a FORTRAN code of the algorithm, references and credits are found at the following url: http://www.netlib.org/gcv/gcvspl). By following baseline correction proposed by Le Losq et al. (2012) it is possible to quantify water content in silicate glasses and melts reasonably accurately.

The procedure can also be applied to investigate other volatiles such as sulfate, CO_2, and N_2, in silicate glasses.

7.2 Nucleation and growth

Raman spectroscopy is also a powerful tool to investigate nucleation and growth. For example, recently, De Ligny and Neuville (2017) have shown several examples, in particular in the framework of the nuclear waste storage. Indeed, a possible solution for long-term storage could be the use of a glass ceramic in which the fission products and minor actinides are concentrated in crystals within a glass matrix. This solution would take advantage of the better stability of the crystal and the easy processing of glasses. In a first step, all the elements would be dissolved in the liquid state then quenched. In a second step, crystals would be nucleated and grown by heat treatments. Knowledge of the optimal process parameters, time and temperature, are needed and *in-situ* experiments are highly suitable for determining these parameters (Putnis, 1992). For example, by looking at a borosilicate glass composition with around 4 mol% of Nd_2O_3 (a good candidate to simulate nuclear waste encapsulation material) such crystallization can be observed directly by doing HT *in situ* experiments. Some silico-apatite ($Ca_2Nd_8[SiO_4]_6O_2$) was crystallized within the glass during isothermal heat treatments. The Pt-Rh10% heating wire was used to quench the glass and perform the heat treatments (see Neuville et al. 2014). Its very low thermal inertia allowed very quick temperature equilibration (De Ligny and Neuville, 2017; Neuville and Cormier, 2017).

Conclusion

Raman spectroscopy is a powerful tool to investigate mineral, gases, glasses, and disordered materials at room temperature, high temperature, high pressure or in all in-situ conditions. It is also possible by coupling Raman spectroscopy with a high-pressure apparatus or high temperature device, it is also possible to investigate the structure of materials *in-situ* conditions and to follow phase transformations and thermodynamic processes. During a long time Raman spectroscopy was confined in research labs. However its non-destructive properties, its long working distance and the lowering of laser prices make it more common nowadays. Indeed, Raman spectroscopy is also now used to investigate quality control during industrial process, make pressure and temperature sensors, follow volatiles speciation in exhaust fume, detect pollutant organic compounds in effluent. and quantification in glasses or fluid inclusions, and organic materials.

Now with new small and compact apparatus, it is possible to make direct Raman spectroscopy analyze on-site, like volcanos, polluted ground on a former industrial site, a picture or a sculpture in museum. Raman spectroscopy is a fantastic tools to investigate material but the absence of real interactive database leads to difficult determination. The RRUFF database is very useful and a big improvement for the mineralogical community. However to use it you need to have an idea of the chemical composition of the compound.

One of the only real problems with Raman spectrometry today is that, overall, Raman spectrometers are cheap, easy to use, and that many users do anything without taking the necessary time to think about the physical measurement they do.

REFERENCES

Agarwal, K. Davis, and M. Tomozawa, Journal of non-crystalline solids 185, 191-198 (1995).

Akagi R, Ohtori N, and Umesaki N, (2001) J Non-Cryst Solids 293/295:471-476

Albrecht MG, Creighton JA (1977) J Am Chem Soc 99:5215–5217

Alessi, S. Girard, M. Cannas, S. Agnello, A. Boukenter, and Y. Ouerdane, J. Light. Technol. 30, 1726 (2012).

Amalberti J., Neuville D.R., Sarda Ph., Sator N., Guillot B. (2011a) Japan Geophysical Union, Tokyo, 22-27 Mai.

Amalberti J., Neuville D.R., Sarda Ph., Sator N., Guillot B. (2011b) Goldschmidt, Prague, 14-19 aout.

Angel SM, Gomer NR, Sharma SK, McKay C (2012) App Spectrosc 66:137-150

Balan E, Neuville DR, Trocellier P, Fritsch E, Muller JP, Calas G (2001) Am Mineral 86:1025-1033

Bancroft M., Nesbitt H.W., Henderson G.S., O'Shaughnessy C., Withers A.C. and Neuville D.R. (2018) Journal of Non-Crystalline Solids. 484, 72-83.

Barbier D., Green M., and Madden S.J., Lightwave Technology, Journal of 9, 715-720 (1991).

Bates D, Quist A . (1972) J Chem Phys 56:1529-1533

Begley, R.F.; Harvey, A.B.; Byer, R.L. (1974). Applied Physics Letters. 25 (7): 387–390

Behrens H, Roux J, Neuville DR, Siemann M (2006) Chem Geol 229:96-113.

Bell RJ, Bird NF, Dean P (1968) J Phys C Solid state 1:299–303

Bell RJ, Dean P (1972) In Douglas RW, Ellis B (Eds.) International Conference on the Physics of Non-Crystalline Solids 3rd. Wiley-Interscience 443–452

Ben Kacem I, Gautron L., Coillot D., Neuville D.R. (2017) Chemical Geology, 461, 104-114.

Berghmans, F., B. Brichard, A. F. Fernandez, A. Gusarov, M. V. Uffelen and S. Girard (2008). An Introduction to Radiation Effects on Optical Components and Fiber Optic Sensors, Dordrecht, Springer Netherlands.

Bidault X., Chaussedent S., Blanc W., Neuville D.R. (2016) Journal of Non Crystalline Solids, 433, 38-44.

Boizot B., Petite G., Ghaleb D., Reynard B. and Calas G., J. Non-Cryst. Solids 243 (1999) 268.

Brawer S A, White WB (1975) J Chem Phys 63:2421-2432

Bridgman and Simon (1953) J Appl Phys 24 (1953);

Brückner R.,J. (1987) Non-Cryst.Solids95–96(Part2)961.

Bucheneau U, Prager M, Nucker N, Dianoux AJ, Ahmad N, Phillips WA (1986). Phys Rev B 34:5665–5673

Cabannes J, Rocard Y (1928) J Phys 10:32-34

Cabannes J, Rousset A (1932). CR Acad Sci 194:79-81

Canning, Somnath Bandyopadhyay, Palas Biswas, Mattias Aslund, Michael Stevenson and Kevin Cook, Chapter 18 : InterChopen edition, 2010

Canning, J.; Stevenson, M.; Bandyopadhyay, S.; Cook, K. (2008). Sensors. 8 (10): 6448–6452.

Chabiron A, Pironon J, Massare D (2004) Contrib Mineral Petr 146:485–492

Champagnon B.,S.Degioanni,C.Martinet, (2014) J.Appl.Phys.116, 123509.

Champagnon B, Martinet C, Coussa C, Deschamps T (2007) J Non-Cryst Solids 353:4208-4211

Champagnon, C. Martinet, M. Boudeulle, D. Vouagner, C. Coussa, T. Deschamps, and L. Grosvalet, J. Non-Cryst. Solids 354, 569 (2008).
Cheng J-X (2004) J Phys Chem B 108:827-840
Chryssikos GD, Kamitsos EI, Patsis AP, Bitsis MS, Karakassides MA (1990) J Non-Cryst Solids 126:42-51
Cialla D, Marz, A, Bohme R, Theil F, Weber K, Schmitt M, Popp J (2012) Anal Bioanal Chem 403:27-54
Cochain B, Neuville D R, Henderson GS, McCammon C, Pinet O, Richet P (2012) J Am Ceram Soc 94:1-12
Cochain B., Neuville D.R., de Ligny D., Malki M., Testemale D., Pinet O., Richet P. (2013) Journal of Non Crystalline Solids. 373–374, 18–27
Cornet, A., Martinez, V., de Ligny, D., Champagnon, B., and Martinet, C. The Journal of Chemical Physics 146, 094504 (2017).
Cohen H. M. & R. Roy, Physics and Chemistry of Glasses, 6 (1965) 149.
Das RS, Agrawal YK (2011) Vib Spectrosc 57:163-–176
De Ligny D. et Neuville D.R. (2017) Raman spectroscopy: a nice tools to understand nucleation and growth mechanism. In "From glass to crystal: nucleation, growth and phase separation, from research to applications " Edited Neuville D.R., Cormier L., Caurant D. et Montagne L, éditeur EDP-Sciences.
Denisov VN, Mavrin BN, Podobedov VB, Sterin KE, Varshal BG (1984) J Non-Cryst Solids 64:195-–210
Denisov VN, Mavrin BN, Podobedov YB (1987) Phys Rep :151:, 1-92
Deschamps T, Martinet C, Neuville DR, de Ligny D, Coussa C, Champagnon B (2009) J Non-Cryst Solids 355:2422-2425
Deschamps T., A. Kassir-Bodon, C. Sonneville, J. Margueritat, C. Martinet, D. de Ligny, A. Mermet, & B. Champagnon. (2013) Journal of Physics: Condensed Matter, 25 025402.
Devine, R.A.B. Nucl. Instrum. Methods Phys. Res 91, 378-390 (1994).
Dianoux A. J., U. Buchenau, M. Prager, and N. Nücker, Phys. BC 138, 264 (1986).
Dingwell,S.L.Webb,Phys.Chem.Miner.16(1989)508.
Dubessy J, Caumon M-C, Rull F (2012) European Mineralogical Union Volume 12 Cambrian Printers, Aberystwyth, UK, 504 pp.
Duverger C., S. Turrell, M. Bouazaoui, F. Tonelli, M. Montagna, M. Ferrarie, Phil. Mag. B 77 (1998) 363.
Eaton S M., Haibin Zhang, Peter R. Herman, Fumiyo Yoshino, Lawrence Shah, James Bovatsek, and Alan Y. Arai, Opt. Express 13, 4708-4716 (2005)
Etchepare J, Merian M, Smetankine L (1974). J Chem Phys 60:1873-1879
Fleischmann M, Hendra PJ, McQuillan AJ (1974) Chem Phys Lett 26:163–66
Fukumi K, Hayakawa J, Komiyama T (1990) J Non-Cryst Solids 119:297-302
Furukawa T, Fox KE, White WB (1981) J Chem Phys 75:3226-3237
Galeener FL (1979) Phys Rev B 19:4292–4397
Galeener FL (1982a) J Non-Cryst Solids 49:53-–62
Galeener FL (1982b) Solid State Commun 44:1037–1040
Galeener FL, Lucovsky G (1976) Phys Rev Lett 37:1474-1478
Galeener FL, Leadbetter AJ, Stringfellow MW (1983) Phys Rev B 27:1052-–1078
Galeener FL, Barrio RA, Martinez E, Elliott RJ (1984) Phys Rev Lett 53:2429-–2432
Galeener FL, Sen PN (1978) Phys Rev B 17:1928-1933
Galeener, D. B. Kerwin, A. J. Miller and J. C. Mikkelsen, Jr, Phys. Rev. B 47 [13], 7760-7779 (1993).

Gavenda, T., Gedeon, O., Jurek, K. J. Non-Cryst. Solids 425, 61-66 (2015).
Gillet Ph, Barrat JA, Deloule E, Wadhwa W, Jambon A, Sautter V, Devouard B Neuville DR, Benzerara K, Lesourd M (2002) Earth Planet Sc Lett 203:431-444
Girard et al., in IEEE Transactions on Nuclear Science, vol. 60, no. 3, pp. 2015-2036, June 2013.
Ishiguro, M. Kyoto and H. Kanamori, U. S. Patent 5163987, 1992.
Kakiuchida, E. Sekiya, K. Saito, and A. Ikushima, Jpn. J. Appl. Phys 42. 2003
Kakiuchida, K. Saito, and A. Ikushima, in Jpn. J. Appl. Phys. 42, (2003)6516
Kim, M. Tomozawa, S. Dubois, and Orcel, Journal of lightwave technology 19, 1155 (2001)
Haidar I., Levi G.; Mouton L.; Aubard J.; Grand J.; Lau Truong S.; Neuville D.R.; Felidj N.; Boubekeur-Lecaque L. (2016) Physical Chemistry Chemical Physics. Physical Chemistry Chemical Physics, 18, 32272–32280.
Haidar I., Aubard J., Lévi G., Lau-Truong S., Mouton L, Neuville D.R., Félidj N. and Boubekeur-Lecaque L. (2015) The Journal of Physical Chemistry C, 119, 23149–23158.
Harris DC, Bertolucci MD (1978) Symmetry and spectroscopy: An Introduction to Vibrational and Electronic Spectroscopy. Oxford University Press, New York, 1978 578pp
Hari Babu, M Lancry, N Ollier, H El Hamzaoui, M Bouazaoui and B Poumellec, Applied Optics 55 (27), 7455-7461 (2016)
Hass M (1969) Solid State Commun 7:1069-1071
Hass M (1970) J Phys Chem Solids 31:415-42
Hayami, H. (1991) "Radiation resistant multiple fiber" U. S. Patent 4988162.
El Hayek R., Ferey F., Florian P., Pisch A. and Neuville D.R. (2017) Chemical Geology, 461, 75-81.
Hehlen B, Courtens E, Vacher R, Yamanaka A, Kataoka M, Inoue, K (2000) Phys Rev Lett 84:5355–-5358
Hehlen B, Courtens E, Yamanaka A, Inoue K (2002) J Non-Cryst Solids 307–-310:87–-91
Hehlen B (2010) J Phys:Condens Matter 22:025401-25411
Heili, B. Poumellec, E. Burov, C. Gonnet, C. Le Losq, D. R. Neuville, and M. Lancry, Journal of Materials Science 51, 1659-1666 (2016).
Helander, Journal of Materials Science 39, 3799-3800 (2004).
Hemley RJ, Mao H K, Bell P M, Mysen BO (1986) Phys Rev Lett 57:747–-750
Henderson G.S, Neuville D.R., Cochain B., and Cormier L. (2009) Journal of Non Crystalline Solids. 355, 468-474.
Henderson G.S., M.E. Fleet, J. Non-Cryst. Solids 134 (1991) 259.
Henderson GS, Fleet ME (1995) Can Miner 33:399-408
Henschel, D. Grobnic, S. K. Hoeffgen, J. Kuhnhenn, S. J. Mihailov and U. Weinand, Trans. Nucl. Sci., 58 [4] 2103-2110 (2011).
Herzberg G (1945a) Molecular spectra and molecular structure. I Spectra of diatomic molecule, Princeton Press. 490 pp
Herzberg G (1945b) Molecular spectra and molecular structure. II Infrared and Raman spectra of polyatomic molecules, Princeton Press. 540 pp
Hibben JH (1933) Raman spectra in inorganic chemistry. Chem Rev 13:345-478
Hibben JH (1936) Raman spectra in organic chemistry. Chem Rev 18:1-231
Hollaender A, Williams JW (1929) Phys Rev 34:380-381
Hollaender A, Williams JW (1931) Phys Rev 38:1739-1744
Jeanmarie DL, Van Duyne RP (1977) J Electroanal Chem 84:120-127

Jin, W., Vashishta, P., Kalia, R. K., & Rino, J. P. (1993). Physical Review B, 48(13), 9359.
Kalampounias AG, Yannopoulos SN, Papatheodorou GN (2006) J Chem Phys 124:014504-014509
Karr C (1975) Infrared and Raman spectroscopy of lunar and terrestrial minerals. Academic Press 350 pp
Kamitsos EI, Karakassides MA, Chryssikos GD (1987) J Phys Chem 91:1067-1073
Kingma KJ, Hemley RJ, Mao H, Veblen D (1993) Phys Rev Lett 70:3927-3932
Kleinman DA, Spitzer WG (1962) Phys Rev 125:16-30
Kojitani H, Többens DM, Akaogi M. (2013) Am Mineral 98:197–-206
Kozanecki M., Duval E., Ulanski J., Boiteux G., (2004) Polymer 45, 3781.
Kravets VG, Kolmykova VY (2005) Opt Spectrosc 99:68-73
Landsberg G, Mandelstam L (1928) Naturwissenschaften 16:557-558
Lazarev AN (1972) Consultant Bureau New-York, 350 pp
Lancry and B. Poumellec, Physics Reports 522, 239-261 (2013)
Lancry, B. Poumellec, J. Canning, K.Cook, J.C Poulin and F. Brisset, Laser Photonics Rev. 7, No. 6, 953–962 (2013)
Lancry, E. Régnier and B. Poumellec, Progress in Materials Science, Volume 57, Issue 1, 63-97 (2012)
Lancry, I. Flammer, C. Depecker, B. Poumellec, D. Simons, P. Nouchi, and M. Douay, J. Lightwave Technol. 25, 1198-1205 (2007)
Lancry, K. Cook, D. Pallarés-Aldeiturriaga, J. M. Lopez-Higuera, B. Poumellec, and J. Canning, in Advanced Photonics 2018 (BGPP, IPR, NP, NOMA, Sensors, Networks, SPPCom, SOF), OSA Technical Digest (online) (Optical Society of America, 2018), paper BM2A.4.
Le Losq Ch, Neuville DR, Moretti R, Roux J (2012) Am Mineral 97:779-791
Le Losq Ch, Neuville DR (2013) Chem Geol 346:57-71
Le Losq Ch., Neuville D.R. (2017) Journal of Non-Crystalline Solids. 463, 175-188.
Le Losq Ch, Moretti R, Neuville DR (2013) European Journal of Mineralogy 25:777-790
Le Losq Ch, Neuville DR, Florian P, Henderson GS, Massiot D (2014) Geochim Cosmochim Acta 126:495-517
Le Losq C, Neuville D.R., Florian P., Massiot D., Zhou Z., Chen W., Greaves N. (2017) Scientific Reports, 7, Article number: 16490, doi:10.1038/s41598-017-16741-3
Le Parc, C. Levelut, J. Pelous, V. Martinez and B. Champagnon, J. Phys.: Condens. Matter. 18, 7507 (2006).
Lenoir M, Grandjean A, Linard Y, Cochain B, Penelon B, Neuville DR. (2008) Cheml Geol 256:316-325
Lenoir M, Grandjean A, Poissonnet S, Neuville DR (2009) J Non- Cryst Solids 355:1468-1473
Lenoir M, Neuville DR, Malki M, Grandjean A (2010) J Non-Cryst Solids 356:2722-2727
Licheron M, Montouillout V, Millot F, Neuville DR (2011) J Non Cryst Solids 257:2796-2801
Li J.H.,D.R.Uhlmann,J.Non-Cryst.Solids3(1970)127.
Long DA (1977) Raman spectroscopy, McGraw-Hill. 276 pp
Long DA (2002) The Raman effect: A unified treatment of the theory of Raman scattering by molecules. J Wiley and Sons, 597 pp
Maker, P.D.; Terhune, R.W. (1965). Physical Review. 137 (3A): 801–818.
Magnien V, Neuville DR, Cormier L, Mysen BO, Richet P (2004) Chem Geol 213:253-263
Magnien V, Neuville DR, Cormier L, Roux J, Pinet O, Richet P (2006) J Nucl Mater, 352:190-195
Malinovsky, VK, Sokolov AP (1986) Solid State Commun 57:757–-761
Manara D, Grandjean A, Neuville DR (2009a) Am Mineral 94:777-784
Manara D, Grandjean A, Neuville DR (2009b) J Non- Cryst Solids 355:2528-2532

Maniu D, Iliescu T, Ardelean I, Cinta S, Tarcea N, Kiefer W (2003) J Mol Struct 651-653:485-488
McMillan P (1984) Am Mineral 69:622-644
McMillan PF (1985) Rev Mineral Geochem. 14:9-63
McMillan PF, Piriou B (1982) J Non-Cryst Solids 53:279–-298
McMillan P Piriou B (1983) J Non-Cryst Solids 55:221–-242
McMillan PF, Wolf GH, Poe BT (1992) Chem Geol 96:351–-366
McMillan PF, Poe BT, Gillet P, Reynard B. (1994) Geochim Cosmochim Acta 58:3653–-3664
McMillan PF Hess AC (1988) Rev Mineral 18:11-61
McMillan PF, Hofmeister AM (1988) Rev Mineral 18:99-159
Majérus, L. Cormier, D.R. Neuville, L. Galoisy, G. Calas, J. Non-Cryst. Solids 354 (2008) 2004.
Martinez V., R. Le Parc, C. Martinet, B. Champagnon, Opt. Mater. 24 (2003) 59.
Matson DW, Sharma SK, Philpotts JA (1983) J Non-Cryst Solids 58:323-352
Masso J. D., C. Y. She, and D. F. Edwards, Phys. Rev. B 1, 4179 (1970).
Meade C., R. J. Hemley, and H. K. Mao, Phys. Rev. Lett. 69, 1387 1992
Meera BN, Ramakrishna J (1993) J Non-Cryst Solids 159:1-1, 6
Metrich N, Allard P, Aiuppa A, Bani P, Bertagnini P, Shinohara H, Parello F, Dimuro A, Garaebiti E, Belhadj O, Massare D (2011) .J Petrol 52:1077-1105
Mihailov, D. Grobnic, C. Hnatovsky, R. Walker, P. Lu, D. Coulas, et al. Sensors. MDPI AG, 2017. 17(12): 2909.
Micoulaut M., L. Cormier, G.S. Henderson, J. Phys.: Condens. Matter 18 (2006) R753.
Minsky M (1961) US-Patent US3013467 (A) Microscopy apparatus ⎯ 1961-12-19
Morana, S. Girard, M. Cannas, E. Marin, C. Marcandella, P. Paillet, J. Perisse, J. -R. Mace, R. Boscaino, B. Nacir, A. Boukenter, and Y. Ouerdane, Opt. Mater. Express 5 [4], 898-911 (2015).
Mulliken RS (1929) Chem Rev 6:503-545
Mulliken RS (1933) Chem Rev 11:347-388
Mysen BO (1999) Geochim Cosmochim Acta 63:95–-112
Mysen BO (2003). Eur J Mineral 15:781-802
Mysen BO, Virgo D (1980) Am Mineral 65:885-899
Mysen BO, Frantz JD (1992) Chem Geol 96:321–-332
Mysen BO, Frantz JD (1993) Eur J Mineral 5:393-413
Mysen BO, Frantz JD (1994a) Contrib Mineral Petrol 117:1–-14
Mysen BO, Frantz, J.D. (1994b) Geochimica et Cosmochimica Acta 58:1711–-1733
Mysen BO, Virgo D, Wendy JH, Scarfe CM (1980a) Am Mineral 65:900–-914
Mysen BO, Seifert FA, Virgo D (1980c) Am. Mineral 65:867–- 884
Mysen BO, Virgo D, Neumann E-R, Seifert FA (1985a) Am. Mineral 70:317–-331
Mysen BO, Carmichael ISE, Virgo D (1985b) Contrib. Mineral. Petrol 90:101–- 106
Mysen BO, Finger LW, Virgo D, Seifert FA (1982) Am Mineral 67:686–-695
Mysen BO, Neuville DR (1995) Geochim Cosmochim Acta 59:325-342
Nasdala L, Brenker FE, Glinnemann J, Hofmeister W, Gasparik T, Harris JW, Stachel T, Reese I (2003) Eur J Mineral15:931-935
Nasdala L, Smith DC, Kaindl R, Ziemann MA (2004) EMU notes in Mineralogy 6:196-259
Nesbitt H.W, O'Shaughnessy C., Bancroft G.M., Henderson G.S., and Neuville D.R. (2018) Chemical Geology. 10.1016/j.chemgeo.2018.12.009
Nesbitt, H.W., Neuville, D.R., Bancroft, G.M., Henderson, G.S. (2019) Chemical Geology

Neuville DR (2006) Chem Geol 229:28-42
Neuville DR, Mysen BO (1996) Geochim Cosmochim Acta 60:1727-1737
Neuville D.R. et Cormier L. (2017) EDP-Sciences.
Neuville DR, Cormier L, Massiot D (2004) Geochim Cosmochim Acta 68:5071-5079
Neuville DR, Cormier L, Massiot D (2006) Chem Geol 229:173-185
Neuville DR, Cormier L, Montouillout V, Florian P, Millot F, Rifflet JC, Massiot D (2008) Am Mineral 83:1721-1731
Neuville DR, Henderson GS, Cormier L, Massiot D (2010) Am Mineral 95:1580-1589
Neuville D.R., Henderson G.S and de Ligny D. (2014) Advances in Raman Spectroscopy Applied to Earth and Material Sciences. In Henderson G.S, Neuville D.R., Down B. (2014) "Spectroscopic methods in Mineralogy and Material Sciences" Review in Mineralogy and Geochemistry, Vol 78, 509-541.
Nian X., X. Zhisan, T. Decheng, J. Phys.: Condens. Matter 1 (1989) 6343.
Novikov A., Neuville D.R., Hennet L., Thiaudière D., Gueguen Y., Florian P. (2017) Chemical Geology, 461, 115-127.
Ollier, N., Piven, K., Martinet, C., Billotte, T., Martinez, V., Neuville, D.R., Lancry, M. (2017) J Non-Cryst Solids 476, 81-86.
Ollier N., Lancry M., Martinet C., Martinez V., Neuville D. R. (2019) Scientific Report. doi.org/10.1038/s41598-018-37751-9
O'Shaughnessy C., Henderson G.S., Nesbitt H.W., Bancroft G.M., Neuville D.R. (2017) Chemical Geology, 461, 82-95.
Pasquarello A (2001). Curr Opin Solid St M 5:503–-508
Pasquarello A, Car R (1998) Phys Rev Lett 80:5145–-5147
Perriot, D. Vandembroucq, E. Barthel, V. Martinez, L. Grosvalet, C. Martinet, & B. Champagnon (2006) Journal of the American Ceramic Society, 89, 596–601. https://doi.org/10.1111/j.1551-2916.2005.00747.x.
Phillips JC (1984) J Non-Cryst Solids 63:347–-355
Poumellec, M. Lancry, A. Chahid-Erraji, and P. G. Kazansky, (2011) Opt. Mater. Express 1, 766-782
Primak, W. (1958) Phys. Rev. 110, 1240-1254
Primak W. and Kampwirth R., (1968) Journal of Applied Physics 39, 5651-5658
Raman CV, Krishnan KS (1928) Nature 121:501-502
Rahmani A, Benoit M, Benoit C (2003) Phys Rev B 68:184202
Reinkober O (1911) Ann Phys-Berlin 34:343-347
Rocard Y (1928) CR Acad Sci 190:1107-1109
Roskosz M, Mysen BO, Cody GD (2006) Geochim Cosmochim Acta 70:2902–-2918
Sakaguchi, Electronics and Communications in Japan (Part II: Electronics) 83(2000).
Sakaguchi and S. Todoroki, Applied optics 37, 7708-7711 (1998).
Saito, M. Yamaguchi, A. Ikushima, K. Ohsono, and Y. Kurosawa, Journal of Applied Physics 95, 1733 (2004).
Saksena BD (1940) P Indian Acad Sci A 12:93-138
Scott JF, Porto SPS (1967) Phys Rev 161:903-910
Seward III T.P., Smith C., Borrelli N.F., and Allan D.C., Journal of non-crystalline solids 222, 407-414 (1997).
Seifert F, Mysen BO, Virgo D (1982) Am Mineral 67:696-717
Sen PN, Thorpe MF, (1977) Phys Rev B 15:4030–-4038

She Y, Masso JD, Edwards DF (1971) J Phys Chem Solids 32:1887-1900
Simmons J.H. ,R.K.Mohr,C.J.Montrose,J.Appl.Phys.53(1982)4075.
Simon G, Hehlen B, Courtens E, Longueteau E, Vacher R (2006) Phys Rev Lett 96:105502-105506
Simon G, Hehlen B, Vacher R, Courtens E (2008) J Phys-Condens Mat 20:155103-155110
Sharma SK, Mammone JF, Nicol MF (1981) Nature 292:140–-141
Sharma S.K., D.W. Matson, J.A. Philpotts, T.L. Roush, J. Non-Cryst. Solids 68 (1984) 99
Sharma SK, Philpotts JA, Matson DW (1985) J Non-Cryst Solids 71:403–-410
Sherwood PMA (1972) Vibrational spectroscopy of solids, 1. Cambridge, Cambridge University Press. 560 pp
Shibata N., M. Horigudhi, T. Edahiro, J. Non-Cryst. Solids 45 (1981) 115.
Shuker R, Gammon RW (1970) Phys Rev Lett 25, 222-225
Spaargaren S.M.R. and Syms Richard R.A., Journal of lightwave technology 18, 555 (2000).
Stiles PL, Dieringer JA, Shah NC, Van Duyne RP (2008) Annu Rev Anal Chem 1:601-26
Stockhorst H. ,R.Brückner,J.Non-Cryst.Solids49 (1982)471.
Susman, S., K. J. Volin, D. L. Price, M. Grimsditch, J. P. Rino, R. K. Kalia, P. Vashishta, G. Gwanmesia, Y. Wang, and R. C. Liebermann. Physical Review B 43, no. 1 (1991): 1194.
Sugiura, H., R. Ikeda, K. Kondo, and T. Yamadaya. Journal of applied physics 81, no. 4 (1997): 1651-1655.
Thomas R (2000) Am Mineral 85:868–-872
Thomas SM, Thomas R, Davidson P, Reichart P, Koch-Müller M, Dollinger G (2008) Am Mineral 93:1550–-1557
Tool, Journal of the American Ceramic Society 29, 240-253 (1946).
Tsujimura T, Xue X, Kanzaki M, Walter MJ (2004) Geochim Cosmoschim Acta 68:5081-5101
Tu Q, Chang C (2012) Nanomed-Nanotech 8:545-558
Umari P, Pasquarello A (2002) Physica B 316-317:572-574
Umari P, Gonze X, Pasquarello A (2003) Phys Rev Lett 90:867-755
Vanelstraete, A. and Laermans, C. Phys. Rev. B 38, 6312-6315 (1988).
Verweij H, Boom Hvd, Breemer RE (1977) J Am Ceram Soc 60:529-34
Villars DS (1932) Chem Rev 11:369-436
Virgo D, Mysen BO, Kushiro I (1980) Science 208:1371–-1373.
Wang, N. Tai, K. Saito and A. J. Ikushima, J. Appl. Phys. 98 [2] 023701 (2005).
Warren BE (1934a) Phys Rev B 45:657-661
Warren BE (1934b) J Am Ceram Soc 17:249-254
Webb S.L D.B. Dingwell, J. Geophys. Res. Solid Earth 95 (1990) 15695.
Webb S.L.,D.B.Dingwell,Phys.Chem.Miner.17(1990)125.
Wilson EB, Decius JC, Cross PC (1955) Molecular vibrations, McGraw-Hill, New York 425pp
Yano T, Kunimine N, Shibata S, Yamane M (2003a) J Non-Cryst. Solids 321:147-156
Yano T, Kunimine N, Shibata S, Yamane M, (2003b) J Non-Cryst Solids 321:157-168
Yamaguchi, K. Saito and A. J. Ikushima, Phys. Rev. B 68 [15] 153204 (2003).
Zimmermann, F., Lancry, M., Plech, A., Richter, S., Ullsperger, T., Poumellec, B., Tünnermann, A. and Nolte, S.,. Int J Appl Glass Sci. Vol 8, 233-238 (2017)
Zachariasen WH (1932) J Am Chem Soc 54:3841-3851
Ziegler LD (1990) J Raman Spectrosc 21:769-779
Zhang X, Kirkwood WJ, Walz PM, Peltzer ET, Brewer PG, (2012) Appl Spectrosc 66:237-249

Zotov N. (2001) Journal of Non-Crystalline Solids, 287, 231-236